NavalResearchLaboratory

Washington,DC20375-5320

NRL/FR/7320--99-9643

A Comparison of Wind Stresses Derived from Archived Operational European Centre for Medium-Range Weather Forecasts 1000-mb Winds and Florida State University Pseudo Stresses over the Tropical Pacific Ocean, 1981-1993

BRUCE W. HUNDERMARK

Sverdrup Technology, Inc.
Stennis Space Center, Mississippi

HARLEY E. HURLBURT

Naval Research Laboratory
Stennis Space Center, Mississippi

E. JOSEPH METZGER

Naval Research Laboratory
Stennis Space Center, Mississippi

JAY F. SHRIVER

Naval Research Laboratory
Stennis Space Center, Mississippi

August 31, 1999

REPORT DOCUMENTATION PAGE

Form Approved
OMB No. 0704-0188

1. AGENCY USE ONLY (*Leave Blank*)	2. REPORT DATE	3. REPORT TYPE AND DATES COVERED
	August 31, 1999	Final

4. TITLE AND SUBTITLE

A Comparison of Wind Stresses Derived from Archived Operational European Centre for Medium-Range Weather Forecasts 1000-mb Winds and Florida State University Pseudo Stresses over the Tropical Pacific Ocean, 1981-1993

5. FUNDING NUMBERS

PE: 0602435N
Project No.: R3523
Accession #: - DN153087

6. AUTHOR(S)

Bruce W. Hundermark, Harley E. Hurlburt, E. Joseph Metzger, and Jay F. Shriver

7. PERFORMING ORGANIZATION NAME(S) AND ADDRESS(ES)

Naval Research Laboratory
Oceanography Division
Stennis Space Center, MS 39529-5004

8. PERFORMING ORGANIZATION REPORT NUMBER

NRL/FR/7320--99-9643

9. SPONSORING/MONITORING AGENCY NAME(S) AND ADDRESS(ES)

Office of Naval Research
800 North Quincy Street
Arlington, VA 22217-5660

10. SPONSORING/MONITORING AGENCY REPORT NUMBER

11. SUPPLEMENTARY NOTES

12a. DISTRIBUTION/AVAILABILITY STATEMENT

Approved for public release; distribution is unlimited.

12b. DISTRIBUTION CODE

13. ABSTRACT (*Maximum 200 words*)

Monthly wind stresses are computed from the European Centre for Medium-Range Weather Forecasts (ECMWF) operational 12-hrly global wind analyses. These are compared with wind stresses derived from the Florida State University (FSU) monthly pseudo stresses (observational data) over the tropical Pacific Ocean domain from 1981-1993. The FSU product is used as the standard for comparison because it was derived using the same procedures and data type.

During 1982-1985, ECMWF equatorial trade winds are 25-55% weaker than those from FSU and the wind stress curl is more diffuse in the northern tropical gyre. Stronger topographically-induced wind features occur in the ECMWF product around the Hawaiian Islands and Central American coast. During 1990-1993, equatorial trade wind magnitudes agree to within 20%, primarily due to uncorroborated strengthening of the ECMWF trade winds (a result of ECMWF product modifications). The ECMWF wind stress curl in the northern tropical gyre is more concentrated. The topographically-induced wind features in the ECMWF product around the Hawaiian Islands and along the Central American coast are smaller in size and stronger. The strengthening in these regions is not corroborated by the FSU product.

14. SUBJECT TERMS

Wind set comparison
Surface winds
Wind stress

15. NUMBER OF PAGES

42

16. PRICE CODE

17. SECURITY CLASSIFICATION OF REPORT	18. SECURITY CLASSIFICATION OF THIS PAGE	19. SECURITY CLASSIFICATION OF ABSTRACT	20. LIMITATION OF ABSTRACT
UNCLASSIFIED	UNCLASSIFIED	UNCLASSIFIED	UL

NSN 7540-01-280-5500

Standard Form 298 (Rev. 2-89)
Prescribed by ANSI Std 239-18
298-102

CONTENTS

A Comparison of Wind Stresses Derived from Archived Operational European Centre for Medium-Range Weather Forecasts 1000-mb Winds and Florida State University Pseudo Stresses over the Tropical Pacific Ocean, 1981-1993

1.0 INTRODUCTION

Wind stress forcing plays an important role in the dynamics of the ocean circulation. The wind stress drives ocean currents and is required as a surface boundary condition for ocean circulation models. Consequently, spurious wind stress forcing can contribute to errors in ocean model simulations, making accurate wind stress fields vital to ocean modelers (Hurlburt et al. 1996b). So far, ocean modelers have primarily used monthly wind stress climatologies constructed from marine surface observations (mainly from ships of opportunity) to provide the wind forcing for their ocean models. The Hellerman and Rosenstein (HR) monthly wind stress climatology (HR 1983) is the one most widely used in the ocean modeling community. In recent years, however, ocean modelers interested in interannual variability and nonclimatological model-data comparisons have also been using wind analyses from various meteorological centers. For example, monthly or daily mean wind stress fields computed from the archived operational European Centre for Medium-Range Weather Forecasts (ECMWF) 1000-mb 12-hrly global wind analyses have been used to provide interannual forcing for the NRL Layered Ocean Model (NLOM) (Hogan et al. 1992; Hurlburt et al. 1992, 1996a,b; Metzger et al. 1992, 1994; Thompson et al. 1992; Jacobs et al. 1994, 1996; Mitchum, 1995; Mitchell et al. 1996; Silivra et al. 1997; Smedstad et al. 1997; Spiesberger et al. 1997, 1998; Fabrikant et al. 1998; Hurlburt and Metzger, 1998). However, spurious trends in the wind fields due to changes in the analysis/forecast system and sparser input data for 12-hrly analyses than available for monthly analyses can cause spurious anomalies and trends in ocean model simulations. The archived operational ECMWF 1000-mb winds were used as the model forcing in the papers just cited instead of the other archived operational ECMWF wind products (10-m winds and direct surface stresses) for three reasons. First, the 1000-mb winds provide the longest time series, starting in Jan 1980 versus Jan 1985, for the other two products; however, 1980 is omitted because of "unrealistic" trends during that year. Second, the direct surface stresses are quite different from the other products near continental boundaries. Third, Ly et al. (1992) have shown that these three products are essentially the same (except as just noted) if multiplied by an appropriate constant.

Several studies have assessed the ECMWF wind product. These studies mainly have compared various operational wind products and satellite-derived winds with the ECMWF winds. Ly et al. (1992) compared the annual and monthly mean wind stress and wind stress curl from HR and from ECMWF 12-hrly operational 1000-mb winds, 10-m winds, and direct surface stress averaged over 1985-1989. Their analyses focused on the western equatorial Pacific and the North Atlantic basin. They found that the wind stresses have similar large-scale patterns but that there are wind stress curl differences (mainly in amplitude) between all the data sets in the Gulf Stream separation region, in the Caribbean, and in the regions of maximum northeast (NE) and southeast (SE) trades. In addition, they found that the global ECMWF 1000-mb wind stress is different from the 10-m wind stress by close to a constant multiple.

Various studies have compared the ECMWF analyses with the National Centers for Environmental Prediction (NCEP) analyses. Lambert (1988) compared analyses produced by ECMWF and NCEP for each January and July during the period 1980-1984. A "reliability" measure, which compares the variance of the differences to observed variances, was used to assess the analyses. This measure indicated that monthly

Manuscript approved January 25, 1996.

means and daily analyses of the horizontal wind components, temperature, geopotential, and specific humidity are unreliable in the tropics, as well as in parts of the Southern Hemisphere (SH). Reliable monthly means and daily analyses were found in the SH midlatitudes and in the extratropical Northern Hemisphere (NH). In an intercomparison of global analyses from NMC and ECMWF over 1980-1986, Trenberth and Olsen (1988) report that ECMWF and NCEP root mean square (RMS) differences in both the pressure and wind fields are unacceptably large in the equatorial regions. He notes that part of these differences can be traced to problems at NMC. Reynolds et al. (1989) compared surface wind analyses from NMC, ECMWF, and the United Kingdom Meteorological Office against independent wind observations from six buoys in the equatorial Pacific (all within 8° of the equator) during Feb-Jul 1987. Agreement between analyzed values and independent buoy data was poor. The analyzed products agreed better with each other than with the buoy observations.

ECMWF winds have also been compared with satellite-derived winds. Mestas-Nunez et al. (1994) attempted to quantify the absolute accuracy of the ECMWF wind analyses from 1980-1986 by comparing them with global wind stress constructed from Seasat-A Satellite Scatterometer (SASS) data during 1978. Although only 3 mo. of noncontemperaneous scatterometer data (7 Jul-10 Oct 1978) was available from SASS, they cite Chelton et al. (1990), who found that this data was useful for identifying large systematic errors in the HR wind stress climatology particularly at high southern latitudes. After removal of the 1 ms^{-1} bias known to exist in the Atlas et al. (1987) SASS data, Mestas-Nunez et al. (1994) found that the difference between SASS and ECMWF meridional profiles of zonally averaged wind stress exceeded a two-standard deviation range of interannual variability only in the tropics, suggesting an error in one or both of the fields. They cite Davison and Harrison (1990), who state that there is no documented evidence for any geographical dependence of the accuracies of SASS winds that would account for errors in the SASS wind stress magnitudes in the tropics. They conclude that the differences probably arise from errors in the ECMWF wind analyses. They exclude data in the tropics (about 25° S-25° N) from the rest of their study.

Halpern et al. (1994) compared monthly mean 10-m height wind speeds derived from the Special Sensor Microwave-Imager (SSM/I) data with monthly mean 10-m winds from the ECMWF analyses between 60°S and 60°N during 1988-1991. The SSM/I data were uniformly processed and were used as the reference dataset to assess the impact of ECMWF operational changes upon the ECMWF 10-m wind speed over the ocean. They found that ECMWF wind speeds were significantly lower than SSM/I wind speeds in the tropics. In addition, they found that tropical wind speed differences became significantly smaller with time; SSM/I wind speeds decreased while ECMWF wind speeds increased. They note that the apparent improvement of the ECMWF wind speeds occurred during the transition from La Nina to El Nino conditions; a time marked by a decrease in the equatorial Pacific wind speed. Halpern et al. (1994) suggest that as a consequence of the ECMWF model changes, the time series of ECMWF surface wind speeds masked the real trend in equatorial Pacific wind speeds during 1988-1991.

Rienecker et al. (1996) compared four surface wind products over the North Pacific Ocean over 1985-1990. These included the SSM/I based winds, the Goddard Earth Observing System (GEOS) wind assimilation product at 10-m, the ECMWF wind analyses at 10-m and the Comprehensive Ocean-Atmosphere Data Set (COADS). In the tropics, the ECMWF stresses are the weakest.

The studies listed above have consistently shown problems in the ECMWF tropical wind analyses and Halpern et al. (1994) has demonstrated a consequence of ECMWF operational model changes on the tropical Pacific wind field. Trenberth (1992) shows, for these analyses, that the monthly mean wind convergence in the equatorial regions is unrealistic when compared with satellite observed outgoing long-wave radiation (OLR), an index of convective activity. Trenberth suggests that some of the problems in the analyzed tropical winds are related to the divergent part of the wind.

In this study, which is similar to Halpern et al. (1994), but uses a longer time series of wind data, monthly wind stresses derived from ECMWF 1000-mb 12-hrly wind components (hereafter referred to as ECMWF wind stress) and Florida State University (FSU) pseudo stress (Stricherz et al. 1992) are compared. The FSU analyses are mainly subjectively analyzed ship winds, but include other data as well. The comparison covers the tropical Pacific Ocean region (124° E-70° W, 29° S-29° N) and spans the period Jan 1981-Dec 1993. The purpose is to assess the ECMWF wind stress over the tropical Pacific Ocean region using a long data record and to examine how the ECMWF and FSU wind stress agreement changes with time. The FSU wind stress is used as the standard for comparison because it was derived using the same procedures and data type throughout the 13-yr. period. As part of this effort, the influence of TOGA (Tropical Ocean Global Atmosphere) TAO (Tropical Atmosphere-Ocean) data (Hayes et al, 1991) on the ECMWF wind analyses in the tropics is discussed. During 1990-1993, ECMWF assimilated TOGA TAO buoy data as part of their analysis system to improve the winds in the equatorial Pacific. By Nov 1992, 80-90% of the buoy data were available via the Global Telecommunication System (GTS) for assimilation (McPhaden, 1995). In addition, trends in the ECMWF and FSU wind stress are compared to test the credibility of trends found in the ECMWF wind stress and to examine the impact of forecast-analysis system changes (hereafter referred to as ECMWF product modifications) upon the ECMWF wind stress during 1981-1993. This study slightly ventures into the ocean response to wind stress forcing and thus should serve as a guide to ocean modelers who are using ECMWF operational winds to force their ocean models.

The outline of this report is as follows. Section 2.0 describes the ECMWF and FSU wind stress data sets, Sec. 3.0 compares the ECMWF and FSU wind stress and wind stress magnitude, while Sec. 4.0 compares the wind stress curl. Section 5.0 presents the results of trend analyses on the ECMWF and FSU wind products and Sec. 6.0 presents a summary and the conclusions from this study.

2.0 DATA

The wind data from ECMWF consists of archived operational global analyses of 12-hrly zonal (u) and meridional (v) wind components at 1000-mb from Jan 1981-Dec 1993 on a 2.5° grid (lat., lon.). Four-dimensional data assimilation was used to produce these analyses (Bengtsson et al. 1982; Hollingsworth et al. 1986). From the velocity components, zonal and meridional wind stress components (τ_x, τ_y) were calculated using the bulk aerodynamic formulae:

$$\tau = \tau(\tau_x, \tau_y) = \rho C_D V(u,v). \quad (1)$$

The surface wind vector V is assumed to be parallel to the surface stress vector. The surface air density is ρ (=1.2 kg/m^3) and the wind magnitude is V. A neutral linear drag coefficient C_D (=1.5 $\times 10^{-3}$) was used. Monthly averaged wind stress components were calculated from the 12-hrly wind stress components and interpolated to a 0.5° grid using cubic splines. The interpolation facilitates comparison with the FSU pseudo stress.

Many changes were made in the ECMWF analysis/forecast system during 1981-1993; these are listed in an ECMWF Technical Attachment (1994). On 21 Apr 1983, a T63 (triangular truncation at wavenumber 63) spectral model replaced a gridpoint model with 1.875° resolution. On 1 May 1985, the horizontal resolution was increased to T106, and on 17 Sep 1991 to T213. The product used in this research was subsampled to 2.5° by ECMWF. Another important change occurred on 2 May 1989, when major modifications were made in the convective parameterization, radiation, and gravity wave drag. These changes contributed to a strengthening of the meridional circulation (Trenberth 1992).

The wind analyses from FSU consist of monthly zonal and meridional pseudo stress components from Jan 1981 - Dec 1993 on a 2.0° grid (lat., lon.). The data encompass the tropical Pacific Ocean region. Pseudo stress components are defined as u*V and v*V (u, v, and V defined as above) and were calculated by FSU primarily from ship wind observations. For this study, the FSU product was converted to a wind stress using the same neutral linear drag coefficient and air density value used for ECMWF and it was interpolated to the same 0.5° grid using a cubic spline interpolator.

3.0 WIND STRESS

The ECMWF and FSU wind stresses were averaged over the 1982-1985 and the 1990-1993 time periods. These two periods were chosen because they encompass the beginning and the end of the wind time series and would help to determine the impact of the TOGA TAO data. The mean wind stress patterns for 1982-1985 are displayed in Fig. 1, while those for 1990-1993 are shown in Fig. 2. The ratio of the wind stress magnitude (ECMWF/FSU) for 1982-1985 and 1990-1993 is shown in Fig. 3. Temporal correlation coefficients calculated at each gridpoint for the 1982-1985 and the 1990-1993 trade wind magnitude time series are shown in Fig. 4. Plots of the ECMWF wind stress in the Pacific Ocean domain (72° S-71° N, 96° E-70° W) and in the Atlantic/Indian Ocean domain (72° S-71° N, 99° W-96° E) are displayed in App. A. Figures A1 and A2 show means over the 1982-1985 and 1990-1993 time periods, respectively.

The ECMWF and FSU wind stress fields contain the prevailing NH and SH subtropical high pressure cells and the associated trade wind systems (Figs. 1 and 2). The trade winds emanate from the eastern sides of the subtropical highs, flow westward and equatorward, and meet in the Intertropical Convergence Zone (ITCZ). The ITCZ is a region of relatively weak winds, while stronger winds are found north and south in the cores of the NH and SH trade winds.

3.1. Equatorial Pacific

During 1982-1985, in the equatorial Pacific and the ITCZ, the ECMWF NE and SE trade winds are 25-55% weaker than the FSU winds (Fig. 3). Several studies report that ECMWF wind speeds in the tropics are too low in comparison with observations (e.g., Trenberth et al. 1990; Halpern et al. 1994). Cross-equatorial flow of the SE trade winds is evident in the eastern Pacific in both wind products, although it is slightly stronger in FSU. This cross-equatorial flow weakens to the west as is seen in other wind climatologies (e.g., Atkinson and Sadler 1970; Atkinson 1971; and Sadler 1975). The dynamics of cross-equatorial flow are discussed by Hastenrath (1985). Along the coast of South America and south of this strong cross-equatorial flow, the ECMWF SE trade winds are twice as strong as the FSU trade winds. The weak equatorial easterlies and strong near-coastal flow produces greater convergence in the southeastern equatorial Pacific in the ECMWF product. In an analysis of ECMWF winds from 1980-1986, Trenberth et al. (1989) and Trenberth (1992) note that convergence south of the equator in the eastern Pacific in the ECMWF product is not expected based on cloud imagery from satellites. He shows that excessive convergence in the ECMWF winds results from difficulties in analyzing the divergent component at low latitudes. In the tropics, the divergent component of the wind assumes much greater importance than at higher latitudes, but tends to be very noisy on a day-by-day basis because of its link with convection, and thus is very difficult to measure and analyze reliably. In the western equatorial Pacific, the trade winds are relatively weak and show closer agreement.

In the eastern equatorial Pacific, the ECMWF-FSU trade wind magnitude temporal correlations are generally less than 0.50 during 1982-1985 and are negative in a small area around 120° W, 5° N. Correlations here are mostly statistically insignificant at the 95% confidence level based on Student's t-test (Fig. 5). The two products also show a marked disagreement in trade wind strength in this region. In the western equatorial Pacific (west of 160° W), trade wind magnitude correlations predominantly range from 0.50-0.70 and are statistically significant.

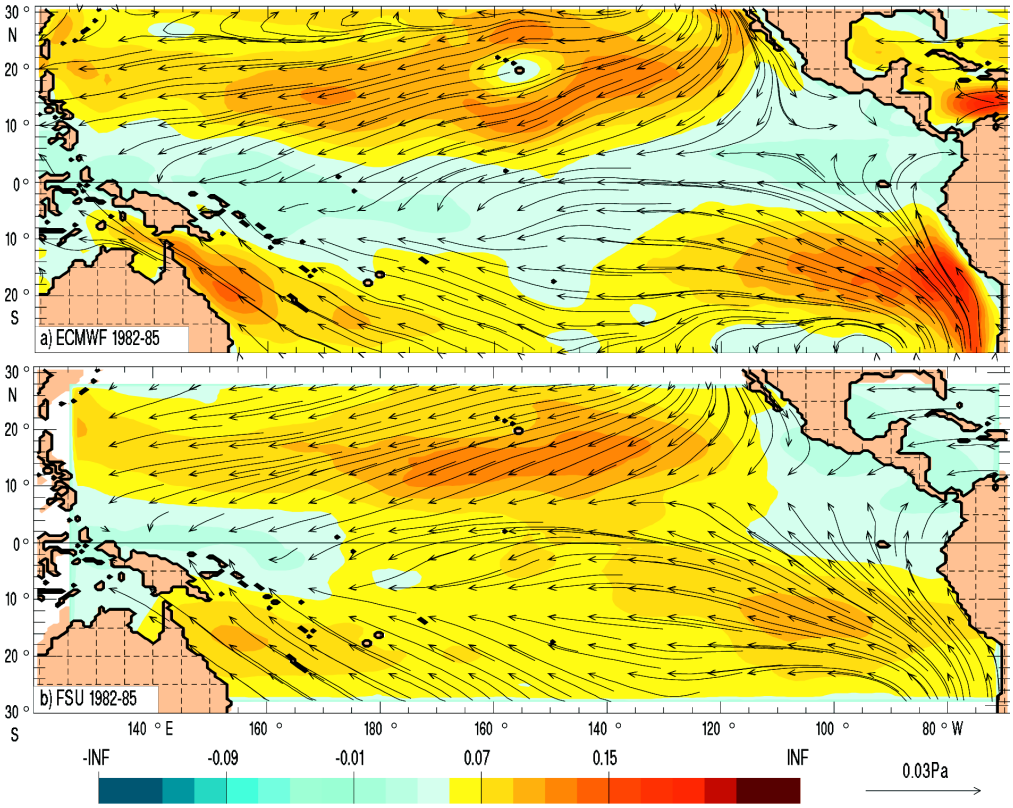

Fig. 1 — Mean wind stress magnitude for 1982-1985 from (a) ECMWF and (b) FSU. Wind stress vectors are overlaid on the wind stress magnitude. The contour interval is 0.020 Pa.

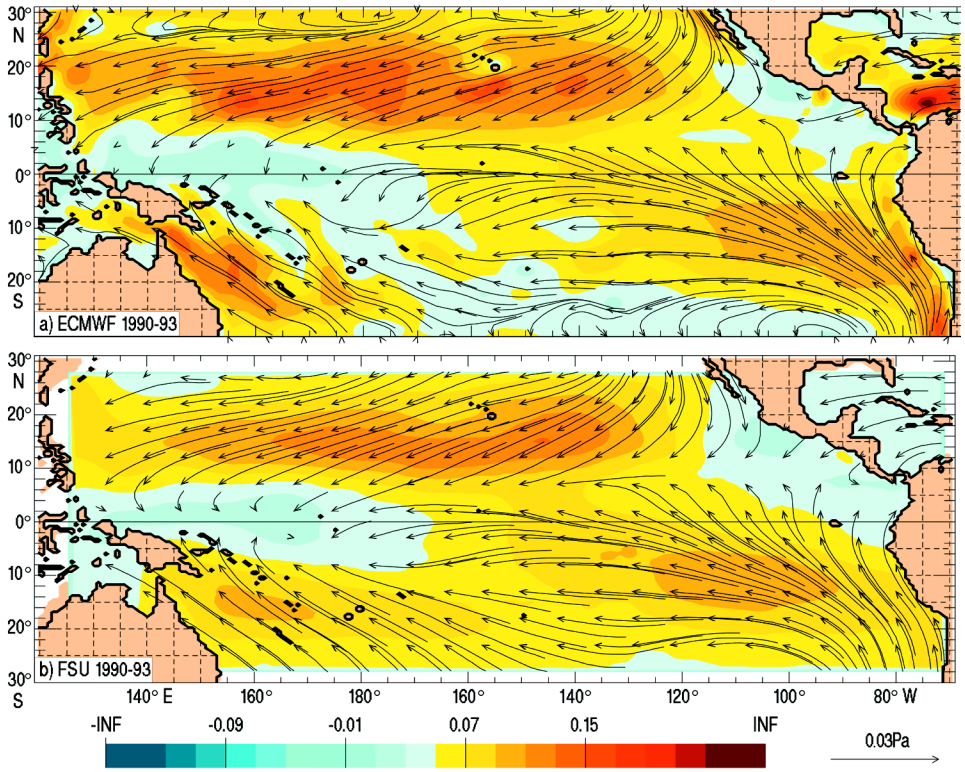

Fig. 2 — Same as Fig. 1, except showing 1990-1993 mean

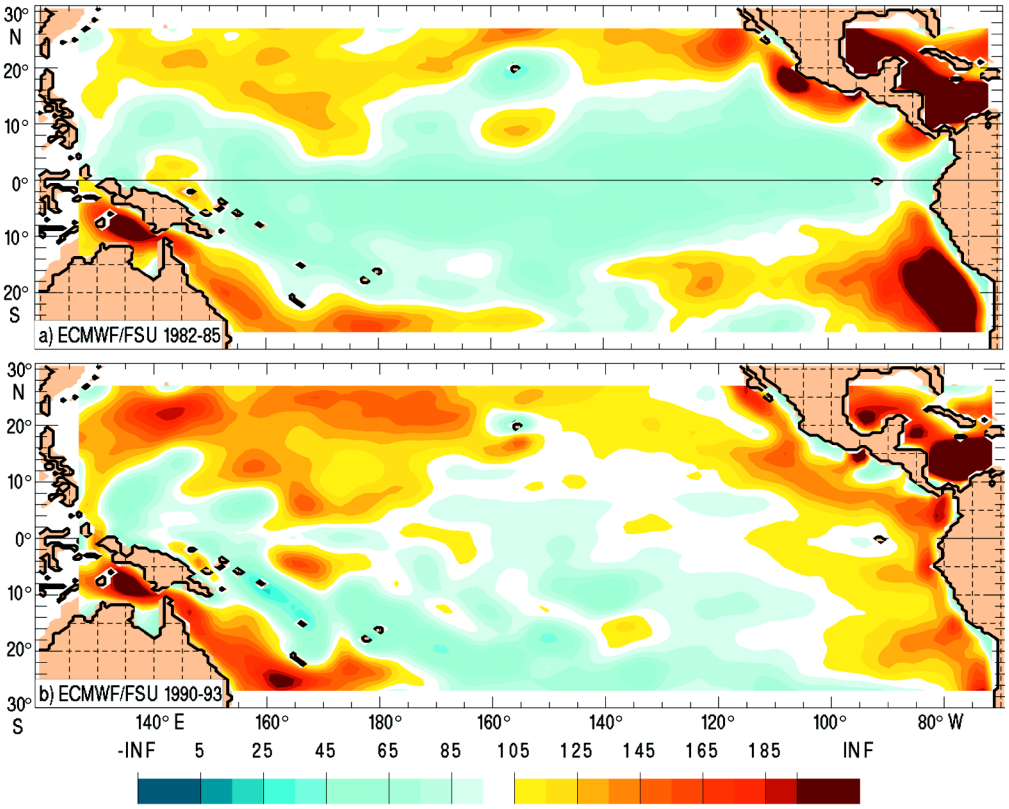

Fig. 3 — ECMWF/FSU wind stress magnitude ratios for (a) 1982-1985 and (b) 1990-1993. Blue shades indicate where ECMWF wind stress magnitudes are weaker than FSU and yellow shades where they are stronger. White indicates equal or nearly equal values. The ratio values are multiplied by 100. The contour interval is 10.

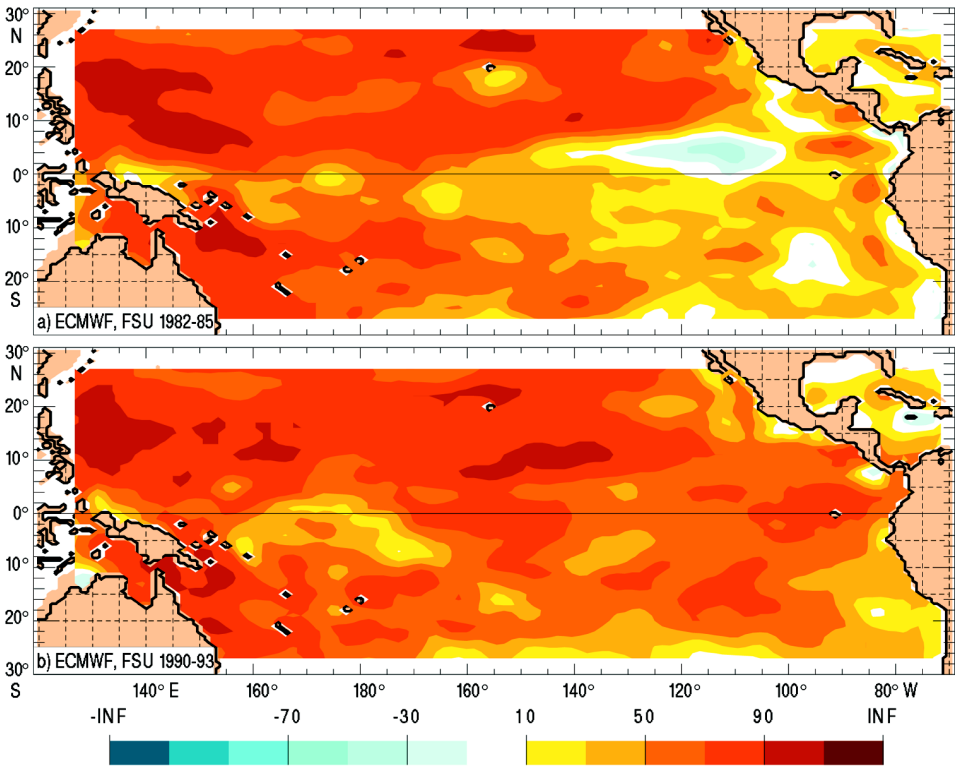

Fig. 4 — Correlation coefficients between the ECMWF and FSU wind stress magnitudes for (a) 1982-1985 and (b) 1990-1993. Yellow shades indicate positive correlations and blue shades indicate negative correlations. Zero or near zero correlations are shown in white. Correlation values are multiplied by 100. The contour interval is 20.

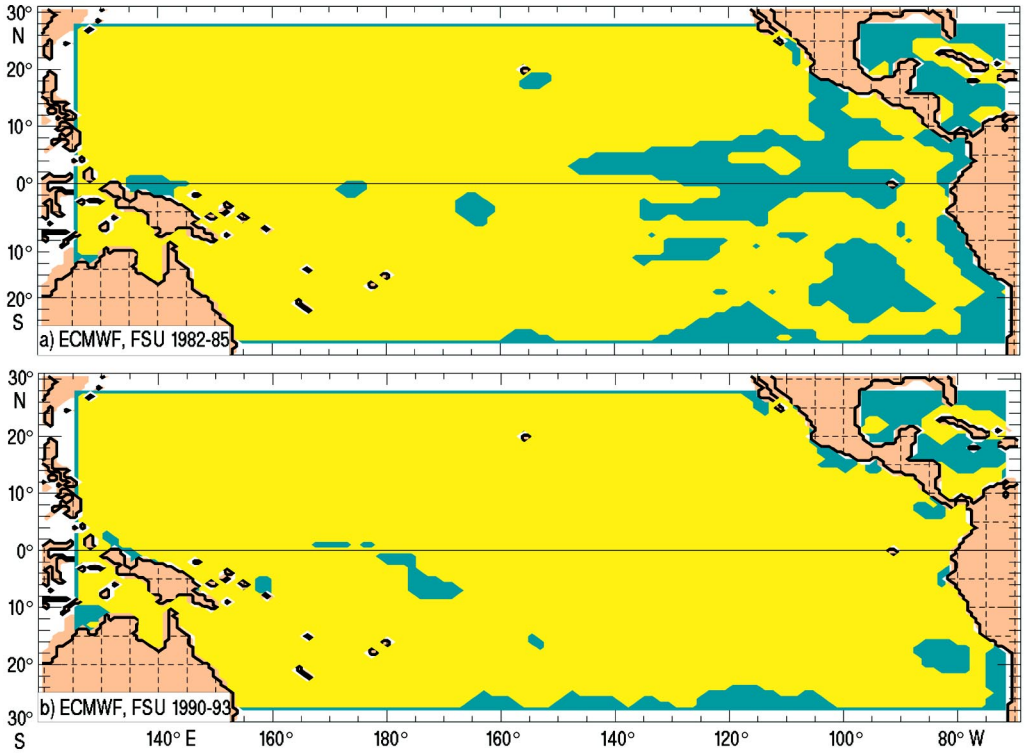

Fig. 5 — Statistical significance of the wind stress magnitude correlation coefficients for (a) 1982-1985 and (b) 1990-1993. The statistical significance was calculated using Student's t test at the 95% confidence level. Yellow indicates statistical significance while blue indicates the correlation is statistically insignificant. A correlation of 0.26 is statistically significant.

During 1990-1993, the ECMWF and FSU equatorial trade wind magnitudes agree more closely primarily due to significant ECMWF trade wind strengthening (Figs. 2 and 3). In the majority of the equatorial Pacific, agreement is within 20%. The ECMWF SE trade winds off the South American coast remain stronger than those from FSU, but the agreement is improved due to ECMWF trade wind weakening. The stronger ECMWF winds near the equator and weaker ECMWF winds along the South American coast (compared to 1982-1985) results in weaker convergence in the southeastern equatorial Pacific in the ECMWF product. This agrees better with FSU and suggests that the divergent wind problem in the ECMWF product has been greatly reduced or eliminated during 1990-1993. The temporal correlations generally range from 0.50-0.70 across the equatorial Pacific and are statistically significant. A marked correlation improvement is evident in the eastern equatorial Pacific compared with 1982-1985. Correlations in the western equatorial Pacific are similar to those during 1982-1985.

The improved equatorial trade wind agreement during 1990-1993 most likely results from the assimilation of TOGA TAO data by ECMWF. The implementation of the T213 model in Sep 1991 (ECMWF 1994) is also a likely contributor. Prior to the TOGA TAO array (Hayes et al. 1991; Halpern et al. 1994; McPhaden, 1995), observations in the equatorial Pacific region available for assimilation, were strongly skewed towards the ship tracks, leaving many gaps in the spatial coverage (Fig. 6). Data were also inconsistent in time. This sparse observational data would limit the ability of the data assimilation scheme to significantly improve the analyses. The addition of TOGA TAO data provided more consistent observational data in space and time for assimilation. The distribution of the TOGA TAO array in the equatorial Pacific is shown in Fig. 6. To examine the influence of TOGA TAO data, the RMS of the wind stress magnitude was calculated in the general TOGA TAO region for each month during 1981-1993 for ECMWF and FSU. These energy values are shown in time series (Fig. 7). While slight improvement in the trade wind agreement is apparent from

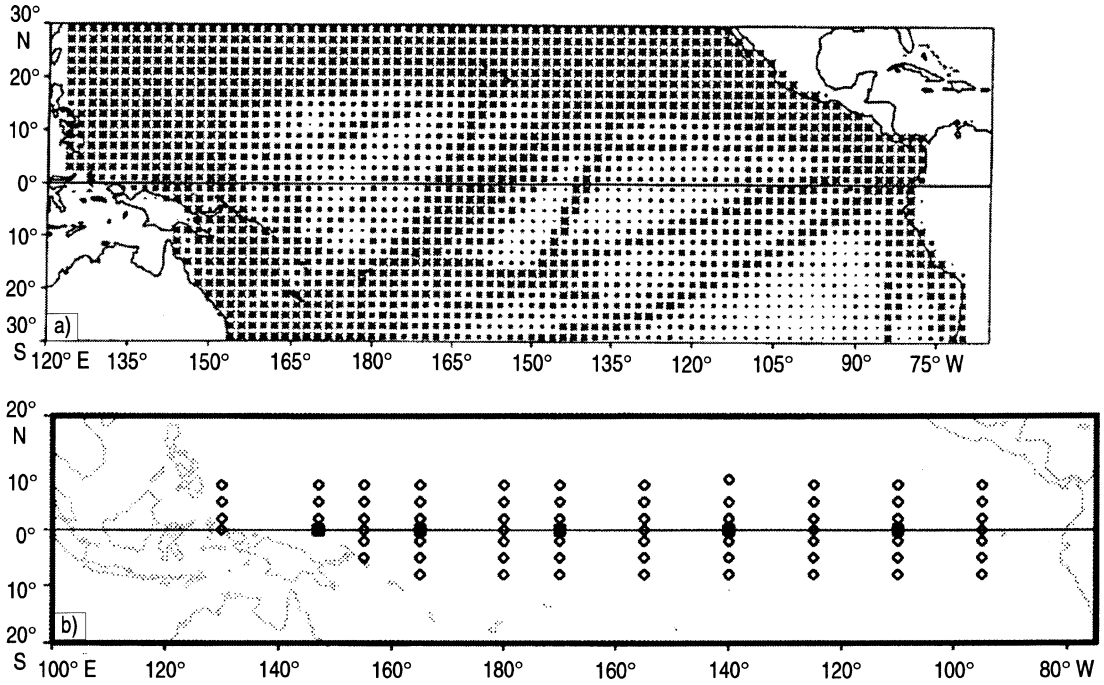

Fig. 6 — (a) The distribution of COADS pseudo stress observations for 1985-1989. (Adapted from Shriver et al. 1993). (b) The TOGA TAO array in the equatorial Pacific (from Hayes et al. 1991).

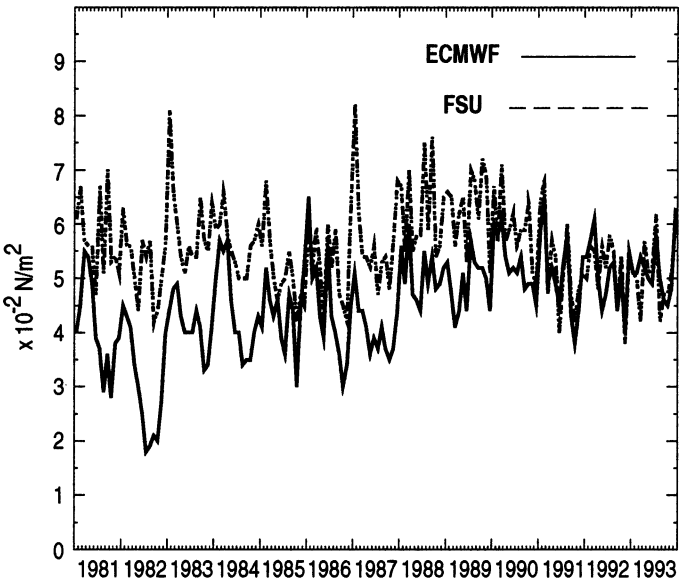

Fig. 7 — The RMS of the ECMWF and FSU wind stress magnitude for the TOGA TAO region. Units are N/m^2 (Pa).

1981-1990, a dramatic improvement occurs in 1991. In addition, correlation coefficients between the ECMWF and FSU trade wind magnitude were computed in the general TOGA TAO region for each year 1981-1993 (Table 1). Prior to 1991, correlations are generally less than 0.70; however, from 1991-1993, correlations are highest and range from 0.73-0.80. Yearly correlation plots also show the much improved trade wind agreement in the equatorial Pacific during 1991-1993 compared to earlier years (Fig. 8). The energy analyses and correlation coefficients show marked improvement in the ECMWF and FSU equatorial trade wind agreement beginning in 1991.

The improved trade wind agreement in the southeastern Pacific off the South American coast cannot be attributed to TOGA TAO data, as this is outside the TOGA TAO region and is not contemperaneous with the addition of TOGA/TAO data in the ECMWF analyses. Timing suggests that it results from ECMWF product modifications in the late 1980's. An ECMWF wind stress magnitude time series at a point off the South American coast shows that improved agreement began in 1985-1986 (Fig. 9). However, the improvement occurs over a long period of time, making it difficult to link this to any one product modification or model physics change. The following major changes might have contributed to the improved agreement. In May 1985, along with the increase in the model horizontal resolution, changes were made in the treatment of clouds, convection, and condensation. In May 1989, as mentioned previously, substantial changes were made to the radiation, cumulus parameterization, and gravity wave drag.

3.2 Subtropical Pacific

During 1982-1985, the ECMWF trade winds are 5-35% stronger than the FSU trade winds in the general region of strongest trade winds. The largest strength differences occur in the western Pacific around 15°-20° N (Fig. 3). Trade wind magnitude temporal correlations in the NH subtropics generally exceed 0.70. In the SH subtropics, they are generally greater than 0.50 in the west and less than 0.50 in the east. Some areas in the east show statistically insignificant correlations (Fig. 5). This correlation pattern shows some relation to the distribution of FSU pseudo stress observations. A comparison of Figs. 4 and 6 generally reveals that areas of high (low) trade wind correlation are consistent with areas containing a high (low) number of pseudo stress observations.

Table 1 — Correlation Coefficients Between ECMWF and FSU Wind Stress Magnitude for the TOGA TAO Region (140° E-95° W, 10° S-10° N)

1982-85	0.61
1990-93	0.74
1981	0.60
1982	0.49
1983	0.62
1984	0.69
1985	0.62
1986	0.65
1987	0.73
1988	0.73
1989	0.68
1990	0.70
1991	0.75
1992	0.80
1993	0.73
1981-93	0.66

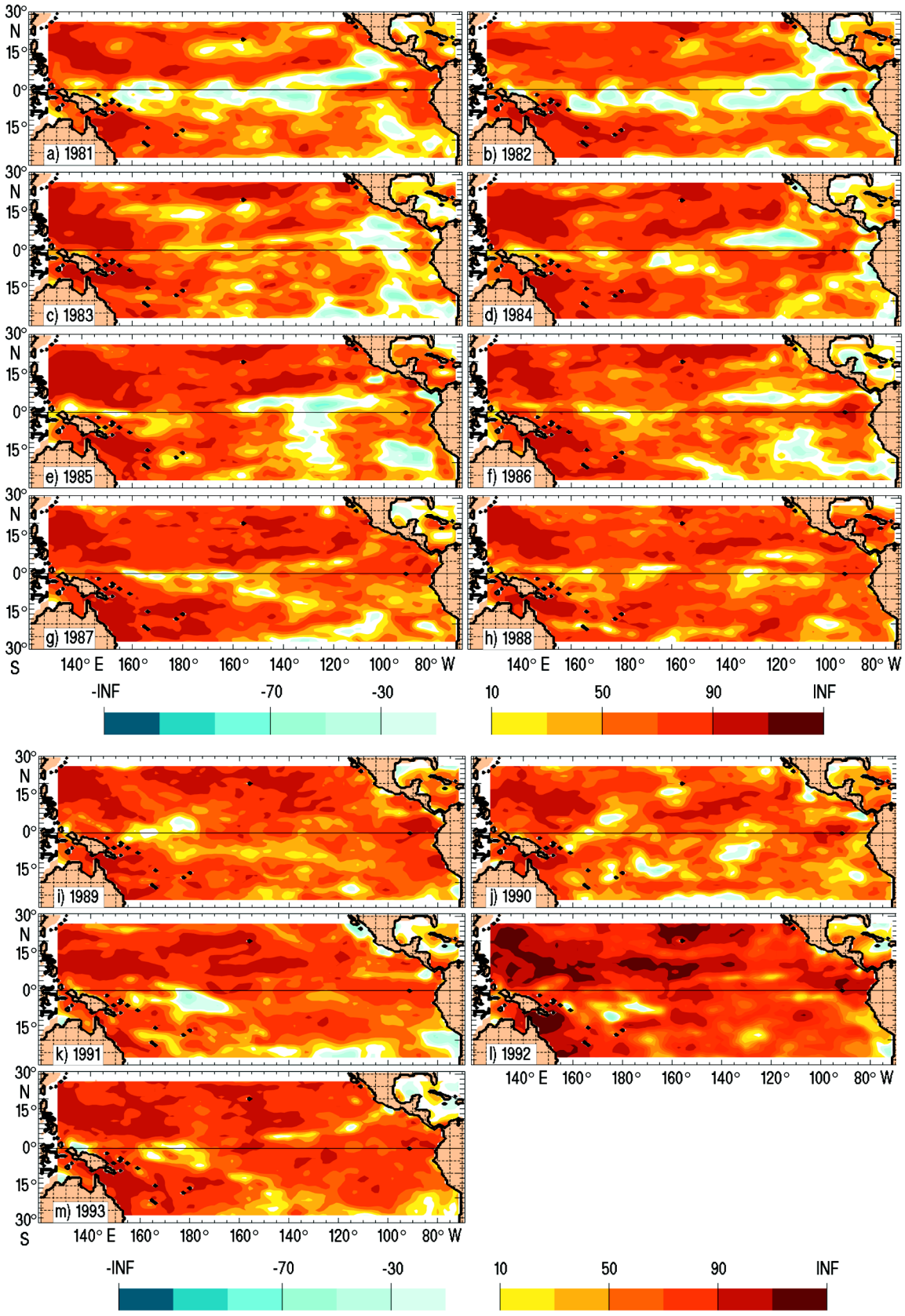

Fig. 8 — Same as Fig. 4, except for (a) 1981, (b) 1982, (c) 1983, (d) 1984, (e) 1985, (f) 1986, (g) 1987, (h) 1988, (i) 1989, (j) 1990, (k) 1991, (l) 1992, and (m) 1993. A correlation of 0.49 is statistically significant.

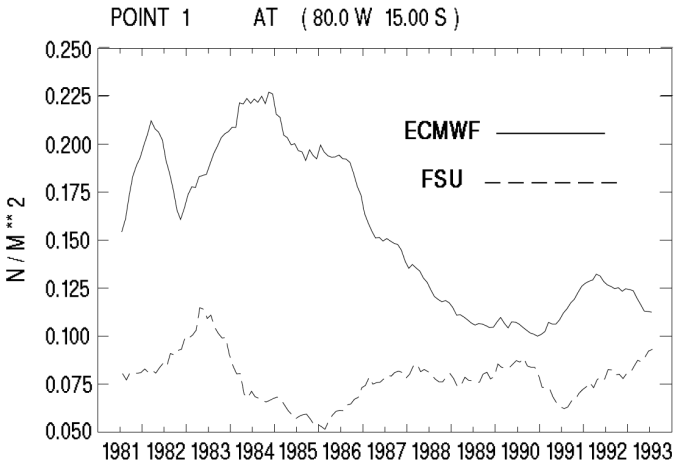

Fig. 9 — Time series of ECMWF and FSU wind stress magnitude at a location along the South American coast (80° W, 15° S) from 1981-1993. The time series are smoothed using a 12-mo running mean filter. Units are Pa.

During 1990-1993, in the NH subtropics, ECMWF trade winds predominantly range from 5-55% stronger, (similar to 1982-85) while towards the SH subtropics, they are weaker by 50% in the interior of the basin but stronger near the coasts of Australia and South America. The pattern of weaker trade winds near the equator and stronger trade winds towards the subtropics is less prominent during 1990-1993 compared to 1982-1985. This can be seen in the yearly ratio plots (Fig. 10). Temporal correlations in the NH subtropical Pacific are similar to those in 1982-1985. Improved trade wind agreement is evident in the eastern subtropical Pacific of the SH where correlations generally range from 0.50-0.70. These higher correlations are associated with the improved agreement in the trade wind strength as discussed in the previous section. Changes with time in the ECMWF and FSU trade wind magnitude agreement outside the equatorial Pacific region are smaller compared to changes within the equatorial Pacific region.

3.3 Effect of the Spatial Variability in the Height of the 1000-mb Surface on the ECMWF 1000-mb/FSU Wind Stress Magnitude Ratio

The ECMWF 1000-mb/FSU wind stress magnitude ratio showed weaker ECMWF equatorial trade winds. However, this analysis compared winds at a generally constant height (FSU product) against those at the varying height of the 1000-mb surface (ECMWF product). Since the height of the 1000-mb surface is generally lower at the equator and higher in the subtropical high pressure belts, the weaker ECMWF equatorial trade winds could have been caused by a depressed 1000-mb surface. To examine this, we compare three maps of wind amplitude ratios: ECMWF 1000-mb/ECMWF 10-m, ECMWF 10-m/FSU and ECMWF 1000-mb/FSU.

Figure 11 shows the ECMWF 1000-mb/10-m wind stress magnitude ratio for the tropical Pacific Ocean domain averaged over 1990-1993. For this map, the ECMWF 10-m winds at each gridpoint are normalized by the spatially averaged ECMWF 1000-mb/ECMWF 10-m wind stress magnitude ratio. To the extent that the normalized ratio in Fig. 11a varies over the domain, the fluctuating height of the 1000-mb surface has impacted the spatial pattern of the ECMWF 1000-mb/FSU wind stress magnitude comparison. The amplitudes differ by less than 5% over most of the tropical Pacific domain, but differ by up to 15% in the equatorial Pacific. This indicates that the ECMWF 1000-mb and ECMWF 10-m winds are not a constant multiple and the varying height of the 1000-mb surface has had some influence on the ECMWF 1000-mb/FSU wind stress magnitude ratio. To test this further, the ECMWF 1000-mb/FSU wind stress magnitude ratio (Fig. 3) is compared with the ECMWF 10-m/FSU wind stress magnitude ratio (with the ECMWF 10-m wind stress

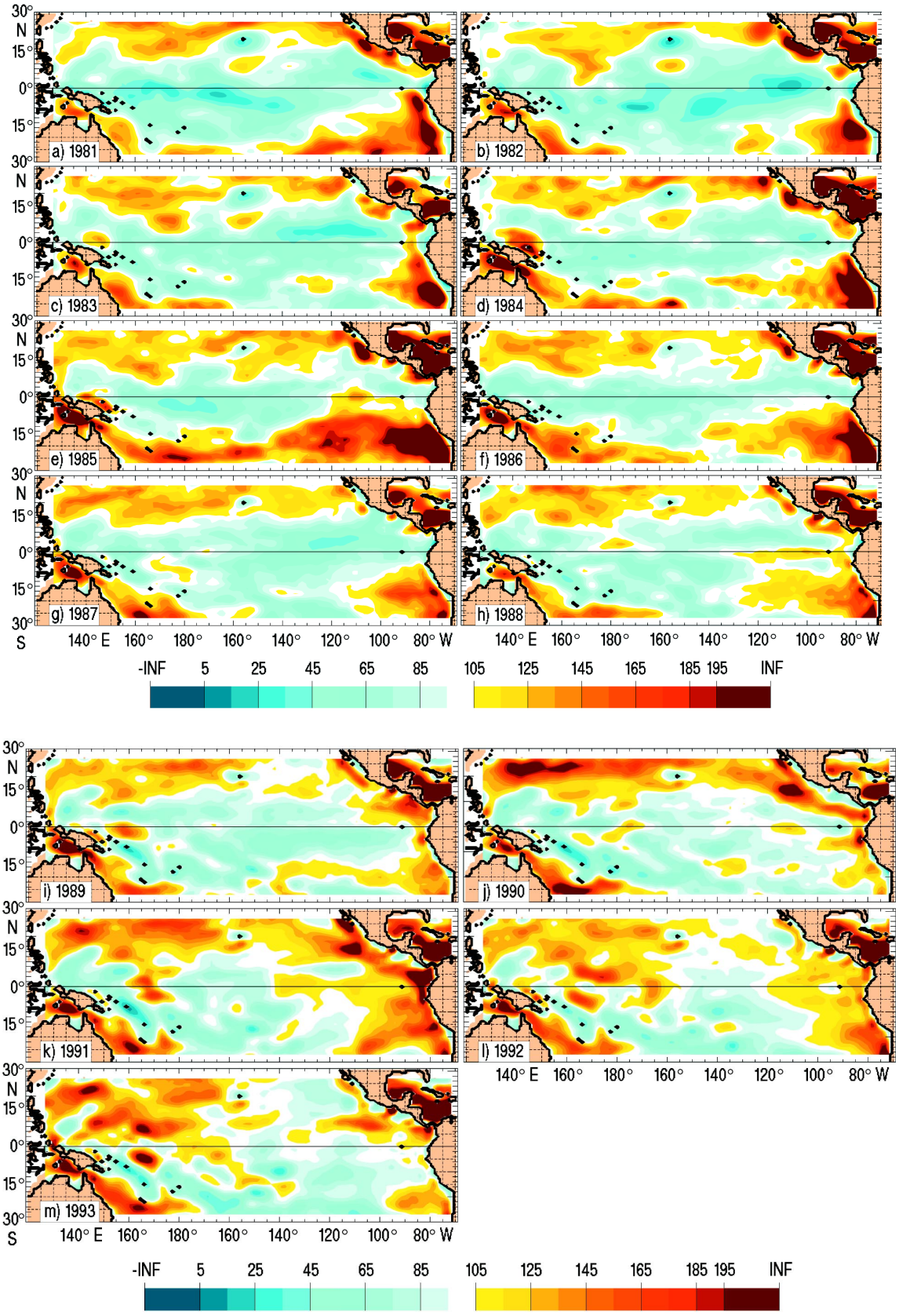

Fig. 10 — Same as Fig. 3, except for (a) 1981, (b) 1982, (c) 1983, (d) 1984, (e) 1985, (f) 1986, (g) 1987, (h) 1988, (i) 1989, (j) 1990, (k) 1991, (l) 1992, and (m) 1993.

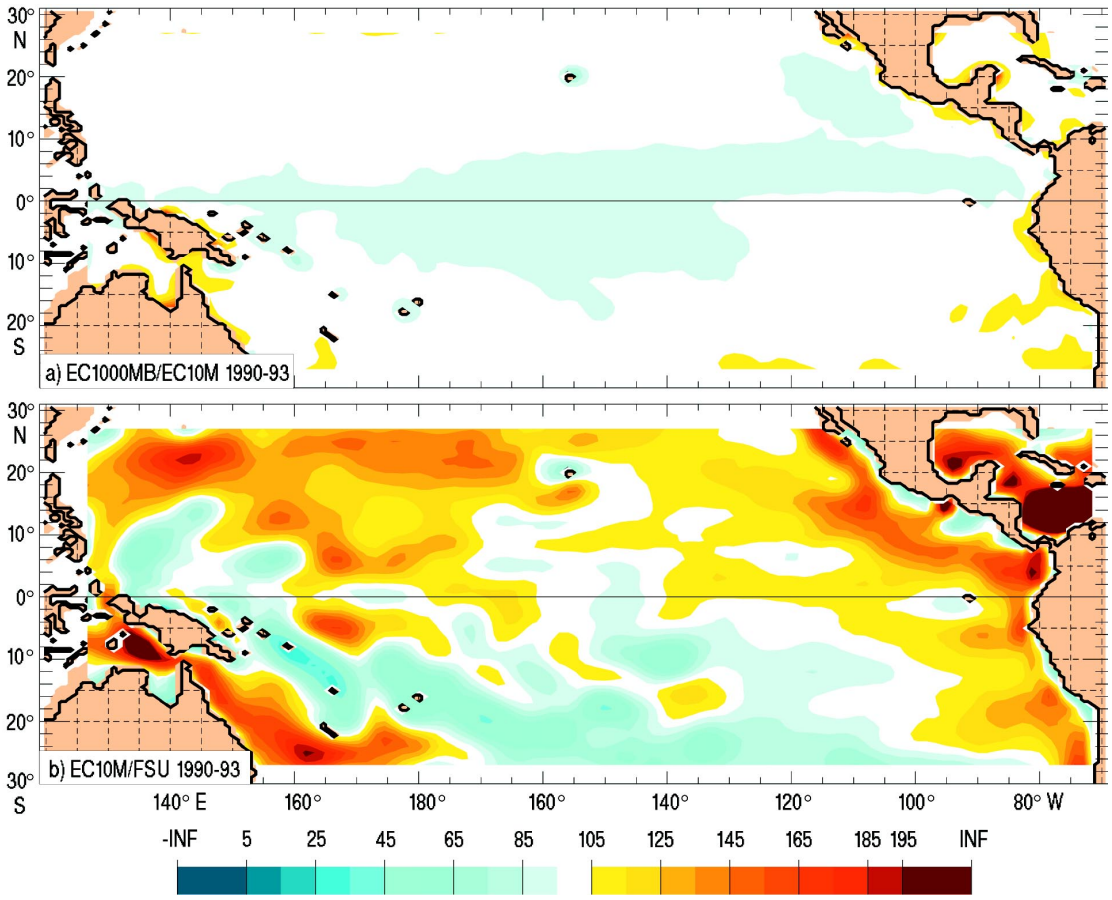

Fig. 11 — The ratio of wind stress magnitudes averaged over 1990-1993 calculated from (a) ECMWF 1000-mb divided by ECMWF 10-m and (b) ECMWF 10-m divided by FSU. For both panels, the ECMWF 10-m winds at each gridpoint were normalized by the spatially averaged ECMWF 1000-mb/ECMWF 10-m wind stress magnitude ratio. Ratio values are multiplied by 100. The contour interval is 10.

magnitude normalized as above) (Fig. 11). If this ratio (comparing two wind sets at a generally constant level) is similar to the ECMWF 1000-mb/FSU ratio (comparing winds with 1000-mb height dependence), then the varying height of the 1000-mb surface is negligible for this study. These ratio patterns are quite similar demonstrating that the ECMWF 1000-mb/FSU wind stress magnitude ratio is not an artifact of the fluctuating height of the 1000-mb surface. The ECMWF 10-m winds could have been used in this study. An ECMWF 1000-mb/ECMWF 10-m wind stress magnitude ratio plot for the global ocean is shown in App. B.

3.4 Influence of Topography

During 1982-1985, the ECMWF NE trade winds partially deflect around the Hawaiian Islands and a local minimum in speed (approximately 65% weaker than FSU) (Figs. 1 and 3) exists. This is due to the significant influence of the Hawaiian Island topography in the ECMWF product; the FSU winds are not as strongly influenced by topography. The influence of the topography in the two products is discussed in Sec. 4.0. The deflection of the winds around the Hawaiian Islands is also noted by Trenberth et al. (1990) in his study of the ECMWF winds. This feature, albeit much weaker, can be detected in the HR and Harrison (1989) climatologies and in the SASS (SEASAT scatterometer) wind stress for Jul-Oct 1978 (Chelton et al. 1990). Topographically-induced wind features off the Mexican and Central American coasts are evident in the ECMWF product because the coastal terrain here is very mountainous. Localized areas of strength

difference are evident off the Mexican coast near 20° N and near the Gulf of Tehuantepec (Fig. 3). Weaker topographical effects are seen in the FSU wind field here. The effects of the topography can be seen much more clearly in the wind stress curl.

During 1990-1993, once again due to the strong topographical influence, the ECMWF NE trade winds deflect around the Hawaiian Islands; however, this feature is smaller in size and stronger due to the ECMWF model resolution increases (Figs. 2 and 3). Likewise, localized areas of strength difference off the coasts of Mexico and Central America are smaller in size. The impact of the ECMWF model resolution increases in these significant topographic regions is discussed in Sec. 4.0.

3.5 Domain Averaged Winds

In the previous sections, emphasis was placed on comparisons with high spatial and low temporal resolution. In this section, domain averaged winds are compared at higher temporal resolution using correlation coefficients and an energy analysis. Yearly correlation coefficients between the ECMWF and FSU wind stress magnitude over the tropical Pacific Ocean domain are shown in Table 2. The best trade wind magnitude agreement occurs near the end of the study period. Correlations range from a low of 0.63 in 1983 to a high of 0.77 in 1992. Over 1981-1993, the correlation is 0.69. The RMS of the wind stress magnitude for each month during 1981-1993 for ECMWF and FSU over the tropical Pacific Ocean domain is shown in Fig. 12. These energy time series show good agreement in phase. ECMWF winds are less energetic in 1981-1982 and generally more energetic beginning in 1983, although differences are small throughout the study period. Since the ECMWF trade winds are generally less energetic than FSU in the equatorial region (Fig. 7), to have nearly equal or greater energy over the tropical Pacific Ocean domain, they must be more energetic than FSU in the subtropical Pacific. This is consistent with the ECMWF/FSU wind stress magnitude ratio results.

4.0 WIND STRESS CURL

The vertical component of the wind stress curl ($curl_z(\tau)$) was computed from the monthly u and v wind stress components using a finite difference approximation. $Curl_z(\tau)$ is an important forcing component of the

Table 2 — Correlation Coefficients Between ECMWF and FSU Wind Stress Magnitude for the Tropical Pacific Ocean Domain

1982-85	0.63
1990-93	0.73
1981	0.64
1982	0.64
1983	0.63
1984	0.66
1985	0.65
1986	0.69
1987	0.75
1988	0.74
1989	0.73
1990	0.68
1991	0.74
1992	0.77
1993	0.75
1981-93	0.69

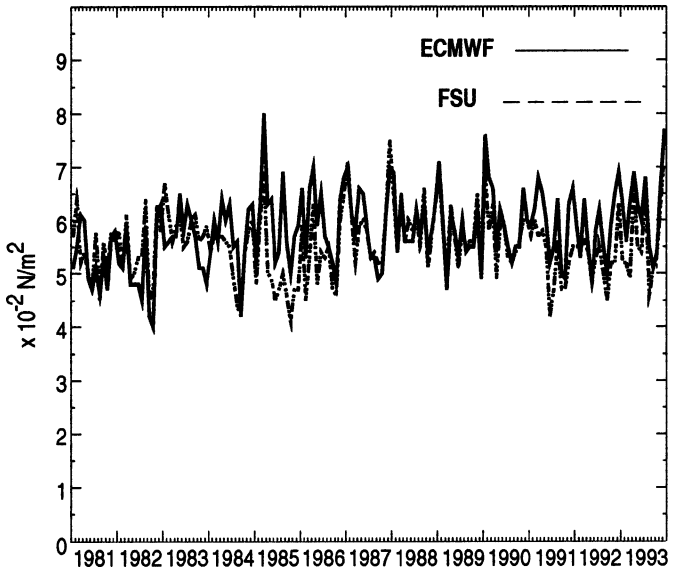

Fig. 12 — Same as Fig. 7, except for the tropical Pacific Ocean domain, 29° S-29° N

ocean circulation because it exerts a torque on the fluid as shown by the vorticity equation. Positive (negative) $\text{curl}_z(\tau)$ imparts cyclonic (anticyclonic) spin to the ocean, which causes divergent (convergent) mass transport in the oceanic Ekman layer. In response to these divergent (convergent) mass transports, an upward (downward) vertical velocity results. This mechanism is known as Ekman suction (pumping) for an upward (downward) induced vertical velocity. In a steady motion of small amplitude, the resultant stretching (compression) of the fluid column results in a poleward (equatorward) motion such that absolute vorticity is conserved. In this situation, the rate at which the fluid column moves poleward (equatorward) to maintain a vorticity balance is given by (2) (Sverdrup, 1947).

$$\beta\rho_w V^* = \text{curl}_z(\tau), \tag{2}$$

where β is the northward gradient of the Coriolis parameter (the beta effect), ρ_w is the density of water, and V^* is the vertically integrated northward volume transport. This is known as Sverdrup flow (e.g., Gill, 1982). It shows that the basin scale, inviscid mass transport is due to planetary vorticity advection driven by the wind stress curl. The Sverdrup relation is obtained by vertically integrating the linearized potential vorticity equation over a constant ocean depth while assuming steady motion and no friction. The Sverdrup relation and the wind stress curl define a mean ocean circulation and current systems, except near the western boundary, because it does not support a western boundary layer to carry the compensating meridional return flow. Zero wind stress curl lines separate northward and southward transports of the subpolar and subtropical gyres, respectively and major zonal currents are often found along latitudes of zero wind stress curl. They are also found where there are strong meridional gradients in $\text{curl}_z(\tau)$ (e.g., the Kuroshio Extension).

Stommel (1948) used the Sverdrup relation with bottom friction and, consequently, showed how the beta effect causes the westward intensification of the ocean currents, and provides a mechanism to close the circulation implied by the Sverdrup flow. Munk (1950) combined the basic features of Ekman, Sverdrup, and Stommel, and added lateral friction and tangential boundary conditions. This allowed a new type of western boundary layer and a relatively complete linear solution for the mean wind-driven ocean circulation that has proved to be quantitatively meaningful in some situations (Godfrey, 1989).

Monthly ECMWF and FSU $curl_z(\tau)$ values were averaged over 1982-1985 and 1990-1993. Results are shown in Figs. 13 and 14, respectively. During both periods, the $curl_z(\tau)$ patterns are generally consistent with the subtropical high pressure cells and the trade wind systems. However, differences exist between the two products. ECMWF $curl_z(\tau)$ for the Atlantic and Pacific domains is shown in App. A. Figures A3 and A4 show means over the 1982-1985 and 1990-1993 time periods, respectively.

4.1 Differences Due to Topography

During 1982-1985, some of the most striking $curl_z(\tau)$ differences between ECMWF and FSU are found around the Hawaiian Islands and along the Central American coast. These differences are due to the stronger topographical influences on the wind field in the ECMWF product compared to the FSU product. The reasons are discussed later in this section. The ECMWF trade winds have strong positive $curl_z(\tau)$ over and north of the Hawaiian Islands and strong negative $curl_z(\tau)$ just to the south (curl dipole). This curl dipole results because the NE trade winds deflect around the islands due to the orography. The FSU trade winds mainly display negative $curl_z(\tau)$ in this region (associated with the NH subtropical high) and do not show the orographic effects as strongly. Similarly, the more detailed ECMWF $curl_z(\tau)$ patterns along the Central American coast result from an orographic effect due to mountainous terrain with gaps.

The ECMWF winds show a greater orographic influence than the FSU winds primarily because the ECMWF model includes topography as a dynamical constraint. Also, the ECMWF data assimilation scheme uses all available data and thus includes sea-level pressure and other data types that the FSU product does not. In addition, in constructing the FSU wind product, the observations are binned over 2° latitude * 10° longitude boxes and then subjectively analyzed to a 2° * 2° grid (Stricherz et al. 1992). Therefore, the FSU winds primarily show synoptic scale features rather than smaller-scale wind features.

During 1990-1993, the curl dipole around the Hawaiian Islands and the $curl_z(\tau)$ features along the coast of Central America in the ECMWF product are smaller in size and stronger due to the ECMWF model resolution increases. In addition, near 155° E, 10° N, the ECMWF trade winds have a “bulls-eye” of positive $curl_z(\tau)$, a feature that was less apparent during 1982-1985 due to the lower model resolution. This $curl_z(\tau)$ feature is maybe due to the effect of Ponape Island on the wind flow. Ponape is located at approximately 158° E, 7° N and has much higher terrain than the surrounding islands and could produce a localized wind pattern.

The effects of the ECMWF model resolution increases can be seen quite clearly in areas of strong topographic influence (e.g. the Hawaiian Islands and Central American coast). When the horizontal resolution increases in the ECMWF model, the spatial scale of topographic wind features decreases. This can be seen most dramatically around the Hawaiian Islands. Figure 15 shows the ECMWF wind stress curl around the Hawaiian Islands averaged over 1982-1985 and 1990-1993. The ECMWF model had higher resolution during 1990-1993. Note how the spatial scale of the curl dipole decreased during 1990-1993 and how it strengthened. A further ECMWF model resolution increase occurred in 1991. Since averaging over 1990-1993 masked this resolution increase, the wind stress curl around the Hawaiian Islands is compared in 1990, 1991, and 1992 (Fig. 16). Between 1990 and 1991, the curl dipole again decreased slightly in size, while not much change occurred between 1991 and 1992. This further decrease in curl dipole size, coinciding with the second increase in the horizontal resolution of the ECMWF model, suggests that the ECMWF product, while depicting the effects of small-scale topographic features, still might not be completely resolving them. This could mean that the resolution is still too coarse to fully resolve these features and/or that subsampling to the 2.5° grid is limiting the effects of the resolution increases in the subsampled product. However, the Hawaiian Islands and the Central American coast illustrate a potential value added by using models to assimilate data, namely, topographic effects, at least when the resolution is sufficient. They also illustrate the effects of resolution in the ECMWF and FSU products.

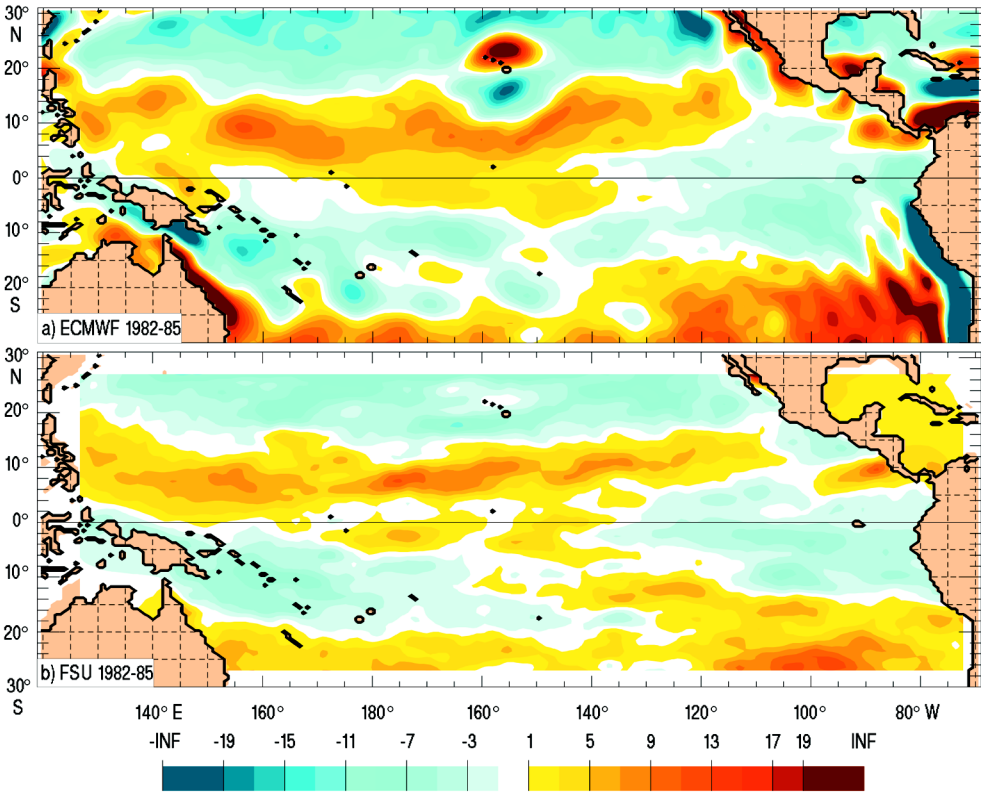

Fig. 13 — Mean wind stress curl for 1982-1985 from (a) ECMWF and (b) FSU. Yellow shades indicate positive wind stress curl and blue shades indicate negative wind stress curl. Zero or near zero wind stress curl lines are shown in white. The values are scaled by 10^{8} on the color bar. The contour interval is $2 * 10^{-8}$ Pa/m.

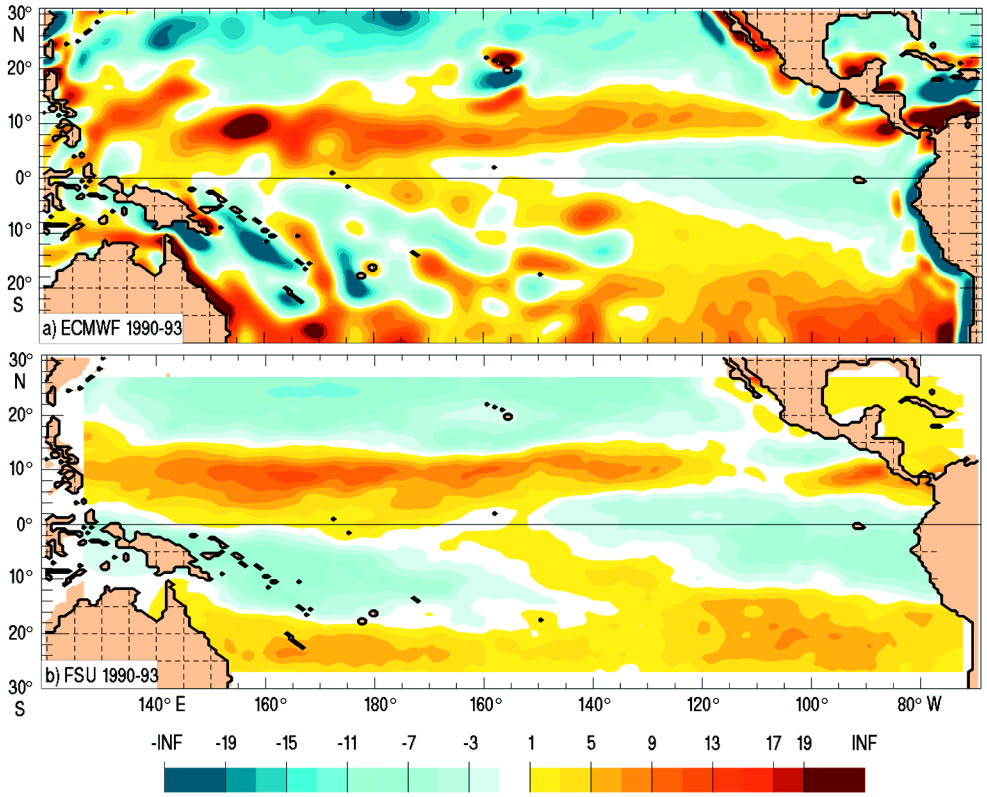

Fig. 14 — Same as Fig. 13, except showing 1990-1993

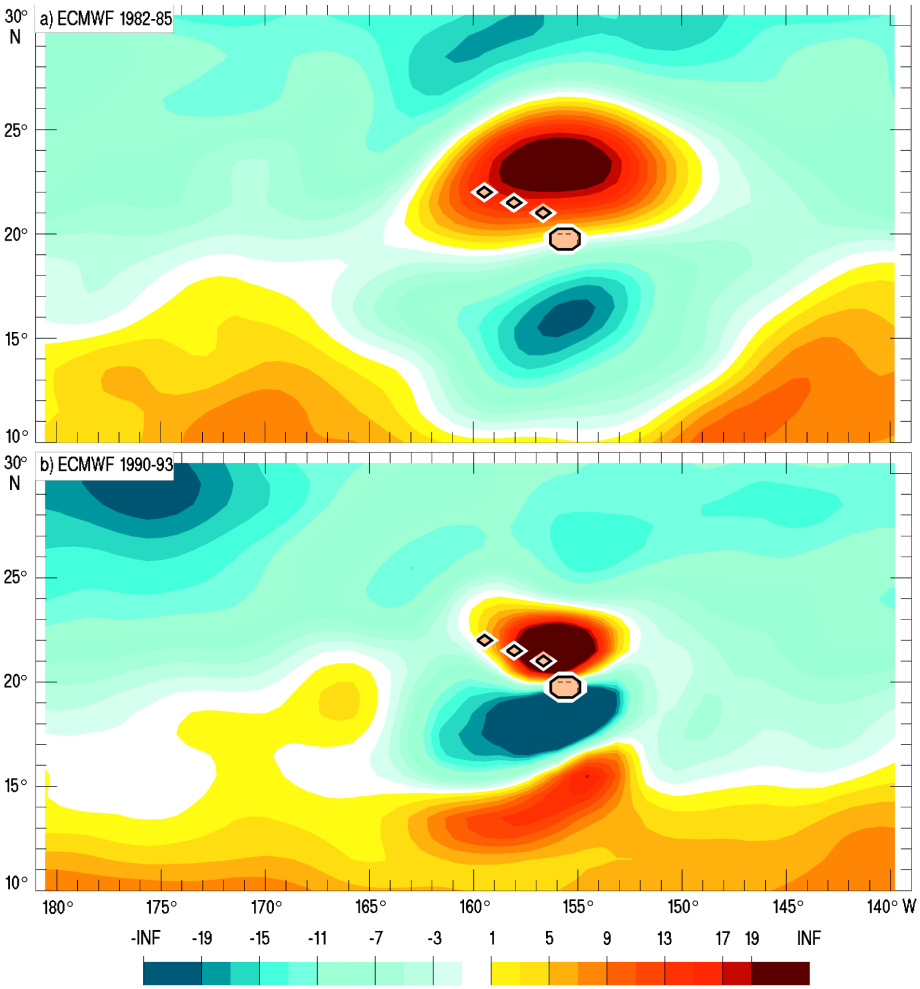

Fig. 15 — Mean ECMWF wind stress curl around the Hawaiian Islands for (a) 1982-1985 and (b) 1990-1993. Yellow shades indicate positive wind stress curl and blue shades indicate negative wind stress curl. Zero or near zero wind stress curl lines are shown in white. The values are scaled by 10^{8} on the color bar. The contour interval is $2 * 10^{-8}$ Pa/m.

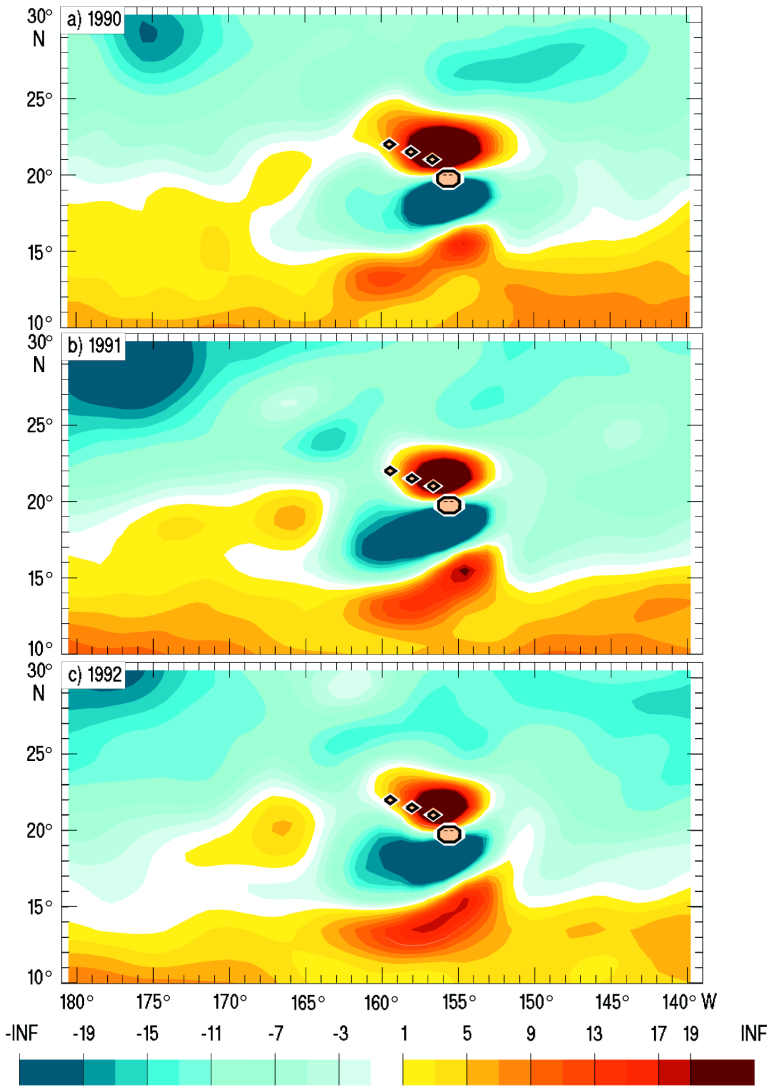

Fig. 16 — Same as Fig. 15, except for (a) 1990, (b) 1991, and (c) 1992

4.2 Other Regions of Differences

A zonal band of positive wind stress curl centered along 10° N spans the Pacific. During 1982-1985, this band of $curl_z(\tau)$ is broader and less zonal in the ECMWF product than in the FSU product. In the ocean, the northern tropical gyre and the currents which bound it on the north, the North Equatorial Current (NEC), and south, the North Equatorial Counter Current (NECC) are forced by this wind curl pattern. The positive $curl_z(\tau)$ west of South America (associated with the SH subtropical high) is stronger in the ECMWF product primarily due to the significantly stronger ECMWF SE trade winds. However, right along the coast, the ECMWF SE trade winds weaken considerably. The resultant strong zonal speed gradient produces negative $curl_z(\tau)$ in the ECMWF product right along the coast. The FSU SE trade winds have a much smaller zonal speed gradient along the South American coast and maintain positive $curl_z(\tau)$ (consistent with the SH subtropical high). In the south central equatorial Pacific (around 10° S-15° S), the ECMWF trade winds have mainly weak negative $curl_z(\tau)$; the FSU trade winds have mainly weak positive $curl_z(\tau)$. The ECMWF negative $curl_z(\tau)$ results primarily from the meridional shear (weak equatorial winds and stronger winds to the south (Fig. 1)). Because the FSU trade winds do not significantly weaken near the equator, they have less meridional shear and maintain positive $curl_z(\tau)$ in this region.

During 1990-1993, the ECMWF and FSU $curl_z(\tau)$ patterns show closer agreement in the northern tropical gyre region (Fig. 14). A much stronger $curl_z(\tau)$ gradient in the ECMWF product compared to 1982-1985 is apparent in this region. The strengthening of the ECMWF winds here had a profound effect on an NLOM simulation that used these winds as forcing, as will be shown in Sec. 5.0. Off the South American coast, weaker SE trade winds in the ECMWF product have decreased the positive $curl_z(\tau)$ (associated with the SH subtropical high) and brought it into better agreement with FSU. However, ECMWF trade winds still weaken toward the coast producing negative $curl_z(\tau)$. In the south central equatorial Pacific, the improved trade wind strength agreement has produced better $curl_z(\tau)$ agreement.

5.0 TREND ANALYSIS

The preceding sections have shown that the ECMWF and FSU wind stress agreement has changed with time, particularly in the equatorial Pacific and west of the South American coast. The ECMWF winds have shown marked changes in these areas over the study period, while the FSU winds have generally shown less change. Therefore, stronger trends would be expected in time series derived from the ECMWF product. To examine the nature of trends in the ECMWF wind stress, linear regression was performed on the ECMWF and FSU wind stress over 1981-1993 and the results compared. The FSU winds were used as the standard for comparison because they were obtained using the same data type and analysis procedures during 1981-1993 (although "unreal" trends are possible in the FSU winds due to increased usage of anemometers on ships instead of the Beaufort scale and an upward trend in their heights (Cardone et al. 1990), changes in ship routes and data errors, and the addition of new data sources like TOGA TAO). Linear regression was performed on each gridpoint of monthly data and the resulting regression coefficients were plotted as maps showing their spatial variations.

For both wind products, the regression coefficients were computed for the wind stress magnitude, the wind stress curl, and for the wind stress components. They were additionally computed for the ECMWF and FSU wind stress differences to more accurately discern spurious linear trends in the ECMWF wind stress. A statistically significant trend in these differences suggests that the trend in the ECMWF product is not real. Differences were calculated by subtracting the FSU analyses from the ECMWF analyses. Therefore, in the simplest scenario, if both wind sets have a collocated strengthening trend, a positive (negative) difference trend indicates a greater (lesser) strengthening trend in the ECMWF wind stress compared to the FSU wind stress. If both wind sets have a collocated weakening trend, a positive (negative) difference trend indicates a lesser (greater) weakening trend in the ECMWF wind stress in relation to the FSU product.

The regression coefficients for the ECMWF and FSU wind stresses and the regression coefficients for their differences are shown in Fig. 17. Their statistical significance is shown in Fig. 18. The regression coefficients for the wind stress curl along with their statistical significance are shown in Figs. 19 and 20, respectively. For the wind stress magnitude, a change of 10^{-4} Pa per month (one contour interval in Fig. 17) represents an approximate change of 10^{-2} Pa over 1981-1993, a typical value for wind stress magnitude. For $curl_z(\tau)$, a change of $5*10^{-10}$ Pa/m per month (one contour interval in Fig. 19) represents an approximate change of 10^{-8} Pa/m during 1981-1993, a typical magnitude for $curl_z(\tau)$. Regression coefficients along with their statistical significance for the ECMWF wind stress and wind stress curl in the Pacific and the Atlantic/Indian Ocean domain are shown in App. C and D, respectively.

5.1 Central and Eastern Equatorial Pacific

In the central and eastern equatorial Pacific, the ECMWF and FSU trade winds and $curl_z(\tau)$ have statistically significant strengthening trends and there is an increase in the meridional gradient of $curl_z(\tau)$. However, the trend in their differences shows that the ECMWF wind product strengthens more, especially in the central equatorial Pacific (similar strengthening occurs in the eastern equatorial Pacific). Therefore, only

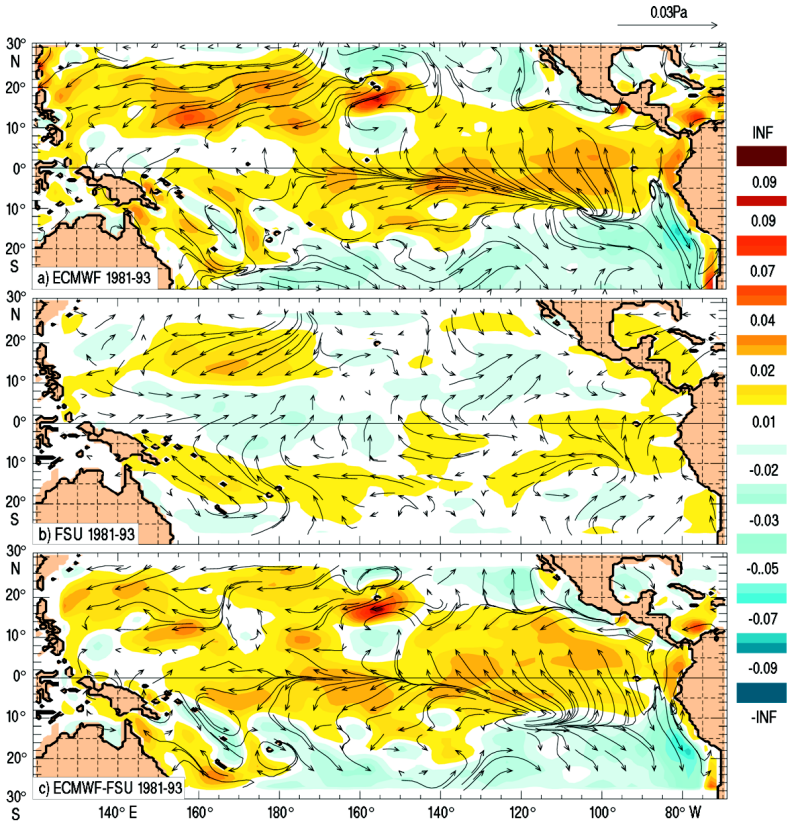

Fig. 17 — Regression coefficients for (a) ECMWF wind stress, (b) FSU wind stress, and (c) ECMWF minus FSU wind stress. The trends in the wind stress magnitude are displayed as color contours. The trends in the wind stress components are shown as the overlaid arrows. Yellow shades indicate a strengthening trend and blue shades indicate a weakening trend. White indicates a zero or near zero trend. The values are multiplied by 100 on the color bar. The contour interval is 10^{-4} Pa/mo.

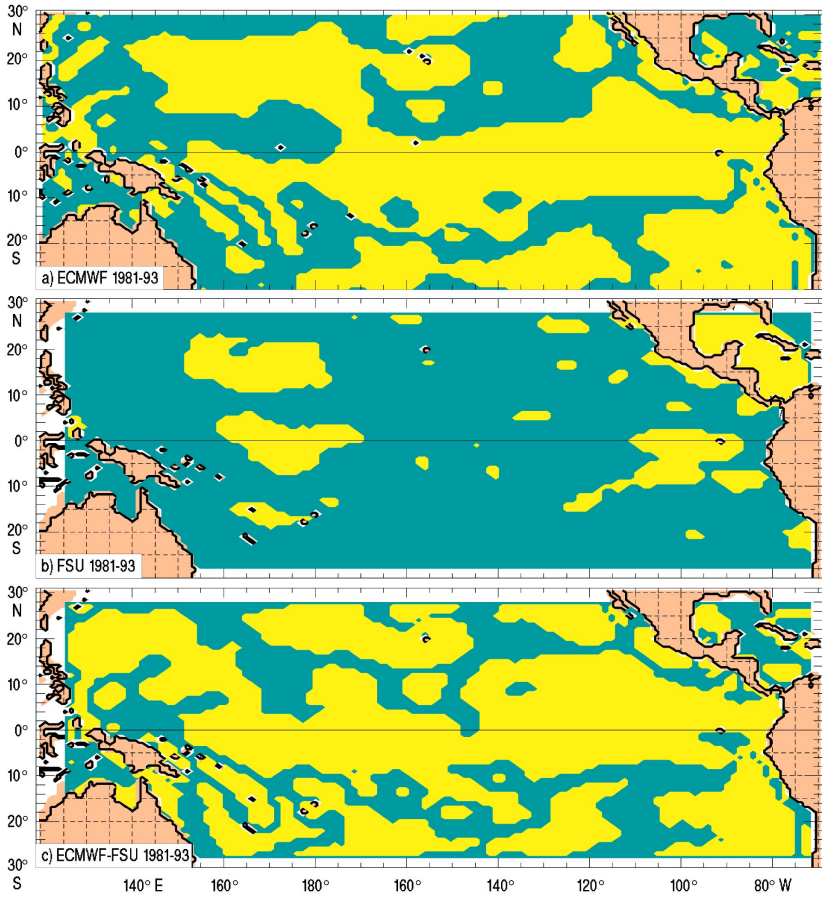

Fig. 18 — Statistical significance of the wind stress regression coefficients for (a) ECMWF, (b) FSU, and (c) ECMWF minus FSU. The statistical significance was calculated using Student's t-test at the 95% confidence level. Yellow indicates statistical significance while blue indicates statistical insignificance.

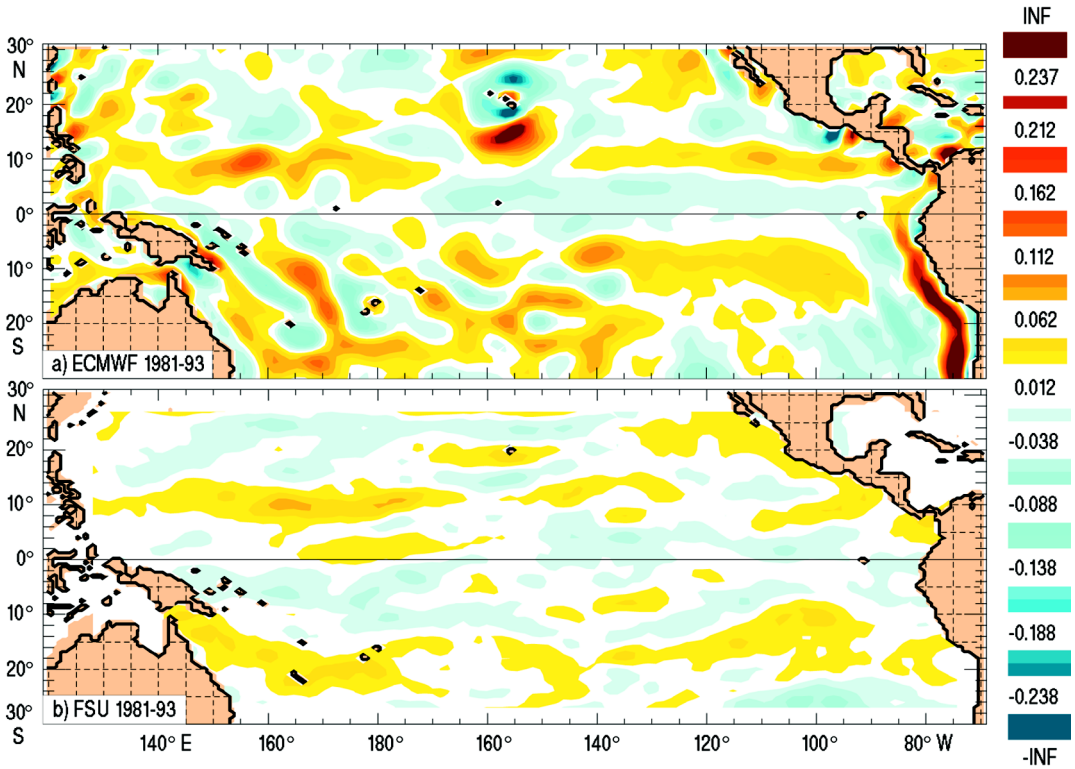

Fig. 19 — Regression coefficients for (a) ECMWF wind stress curl, and (b) FSU wind stress curl. Yellow shades indicate an increasing trend and blue shades indicate a decreasing trend. White indicates a zero or near zero trend. Values are scaled by 10^{8} on the color bar. The contour interval is 2.5 * 10^{-10} Pa/m per mo.

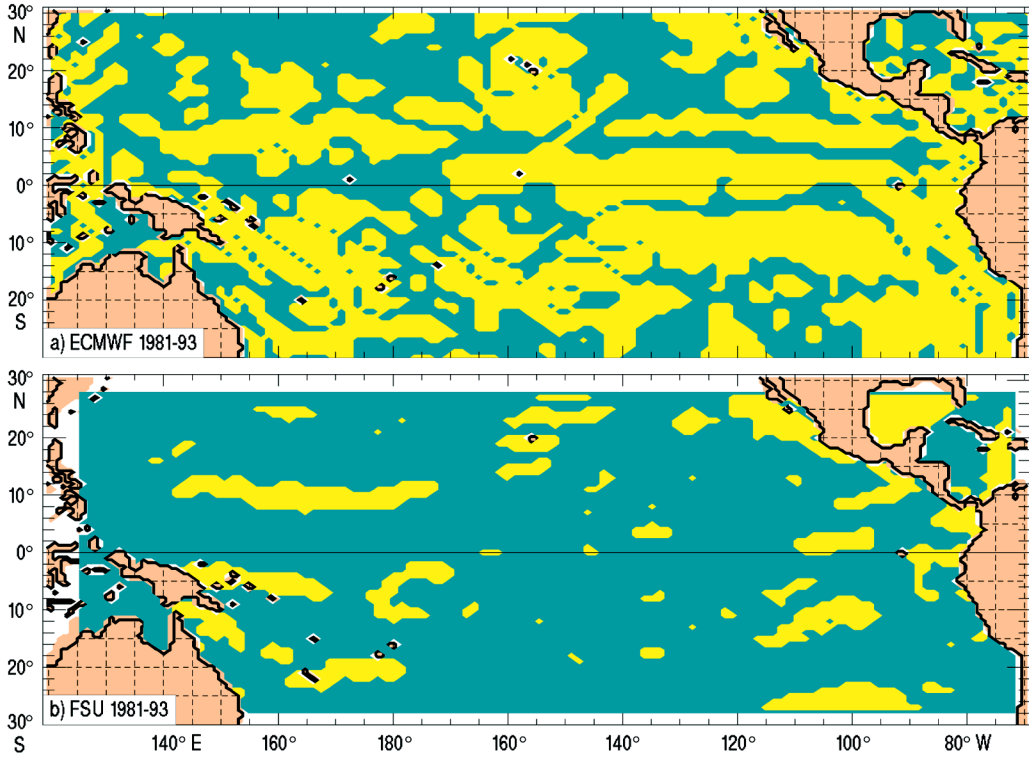

Fig. 20 — Statistical significance of the wind stress curl regression coefficients for (a) ECMWF, and (b) FSU. The statistical significance was calculated using Student's t test at the 95% confidence level. Yellow indicates statistical significance while blue indicates statistical insignificance.

part of the strengthening in the ECMWF trade winds and $curl_z(\tau)$ is real. The excess strengthening results from the use of TOGA TAO data in the analyses and from other product modifications as discussed previously. For example, Trenberth (1992) notes that changes in the convective parameterization and radiation schemes caused a major strengthening of the meridional circulation starting on 2 May 1989. A pronounced strengthening of the ECMWF meridional trade winds is evident near the equator (Fig. 17). Also, the increase to T213 is a likely contributor.

The unreal strengthening in the ECMWF wind product has strongly contributed to the improved agreement between the ECMWF and FSU equatorial trade winds and $curl_z(\tau)$ in the 1990's. Time series of ECMWF and FSU trade winds spatially averaged over the region 180°-100° W, 10° S-5° N (area of most dominant ECMWF trade wind strengthening) during 1981-1993 further illustrate these trends (Fig. 21). The time series are smoothed using a 12-mo running mean filter. The greater strengthening trend in the ECMWF equatorial trade winds is evident; ECMWF trade winds strengthen by about 25% over the 13-yr period, while FSU winds actually weaken in this region by about 15% over 1981-1993 (mainly due to weakening around 160° W-180°). Very close agreement began in 1991. In addition, ECMWF and FSU zonal trade winds spatially averaged over this same region both capture the El Nino events of 1982-1983, 1986-1987 and 1991-1992 (Fig. 21). The El Nino onset is marked by a weakening of the easterlies in the equatorial Pacific. Despite equatorial trade wind magnitude discrepancies between the ECMWF and FSU products, the ECMWF product shows prominent El Nino events in general agreement with the FSU product.

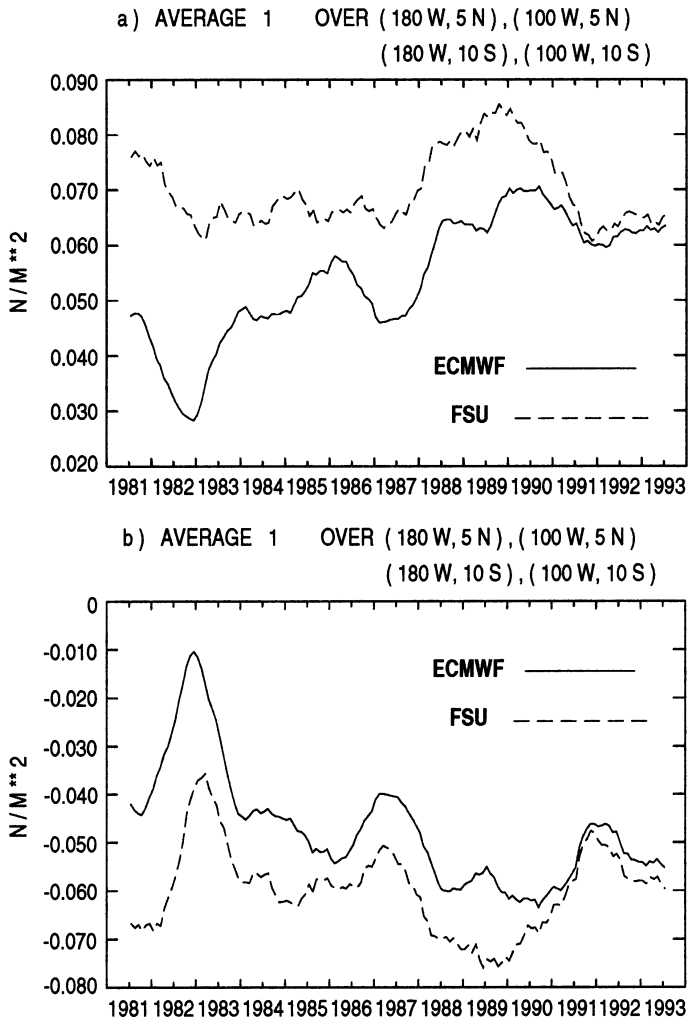

Fig. 21 — Time series of ECMWF and FSU a) wind stress magnitude, and b) zonal wind stress spatially averaged over the region 180°-100° W, 10° S-5° N from 1981-1993. The time series are smoothed using a 12-mo running mean filter. Units are in Pa.

The unreal strengthening of the ECMWF trade winds and $curl_z(\tau)$ in the NECC and northern tropical gyre region and the increase in meridional gradient of $curl_z(\tau)$ across the NECC over 1981-1993 had profound effects on an NLOM simulation forced with a derivative of these winds (hybrid winds). To construct the ECMWF hybrid winds, the ECMWF long-term mean was subtracted and replaced with the HR annual mean. See Metzger et al. (1992) and Hurlburt et al. (1996a) for the reasons for using the hybrid winds. The resultant equatorial easterlies are too weak in the early 1980's and too strong beginning in 1990 (Fig. 9a, Hurlburt et al. 1996a). Sea-surface height (SSH) anomalies and mean SSH averaged over 1982-1985 and 1990-1993 from a 1/8° six-layer Pacific NLOM simulation are shown in Fig. 22. In 1990-1993, the stronger equatorial easterlies caused an eastward strengthening of the northern tropical gyre and a stronger NECC along the southern boundary of the gyre at approximately 5° N. Since strengthening equatorial easterlies were not seen in the FSU product, the strengthening of the northern tropical gyre is not real. Another example is the spurious increase in east-west SSH tilt along the equator (Fig. 22) due to the unrealistic strengthening trend in the equatorial easterlies (Figs. 1, 2, 17, and 21).

These two examples demonstrate the importance of accurate wind forcing for ocean models and show how unreal trends in the wind stress can cause spurious trends in an ocean model. Although no NLOM simulations were forced with the FSU winds (due to their limited areal coverage), the much weaker trends in the FSU winds (Figs. 1, 2, 17, and 21) strongly indicate that the trends in ocean model response discussed above are not, for the most part, due to natural interannual variability. They are even less due to flow instabilities, although flow instabilities with large zonal space scales and long time scales exist in the model, especially in the Kuroshio Extension region (Hurlburt et al. 1996b).

5.2 Western Tropical Pacific

In the western tropical Pacific from about 10°-25° N, the ECMWF and FSU NE trade winds and negative $curl_z(\tau)$ (associated with the NH subtropical high pressure system) have statistically significant strengthening trends. The difference trend shows that the ECMWF wind product strengthens more. In this region, the strengthening in the ECMWF trade winds produces slightly worse ECMWF and FSU trade wind strength agreement in 1990-1993 compared to 1982-1985. In addition, the ECMWF NE trade winds show a local strengthening at 155° E, 10° N (around Ponape Island) not found in the FSU product. The effects of model resolution increases on the wind flow around significant topography is discussed in Sec. 5.4.

5.3 Southeastern Tropical Pacific

Along the coast of South America (10°-30° S) and extending westward to about 180E, the ECMWF SE trade winds and positive $curl_z(\tau)$ (associated with the SH subtropical high) have a statistically significant weakening trend, a trend also seen in the ECMWF-FSU difference. The FSU trade winds have statistically insignificant trends in this region meaning that the ECMWF trends are not real, but an artifact of ECMWF product modifications. It gives improved trade wind magnitude agreement with time and reduces the amount of convergence near the South American coast in the ECMWF product during the 1990's. However, this trend extends too far west, causing slightly worse trade wind magnitude agreement in the central South Pacific during 1990-1993 compared to 1982-1985. The weaker trade wind magnitude has weakened the positive $curl_z(\tau)$ in this region and brought it into closer agreement with FSU. Time series of ECMWF and FSU trade winds further illustrate the trends near the South American coast (Fig. 9).

5.4 Hawaiian Islands

Around the Hawaiian Islands, the ECMWF NE trade wind magnitudes have a statistically significant strengthening trend and a complicated trend pattern of $curl_z(\tau)$ (which is statistically significant). These

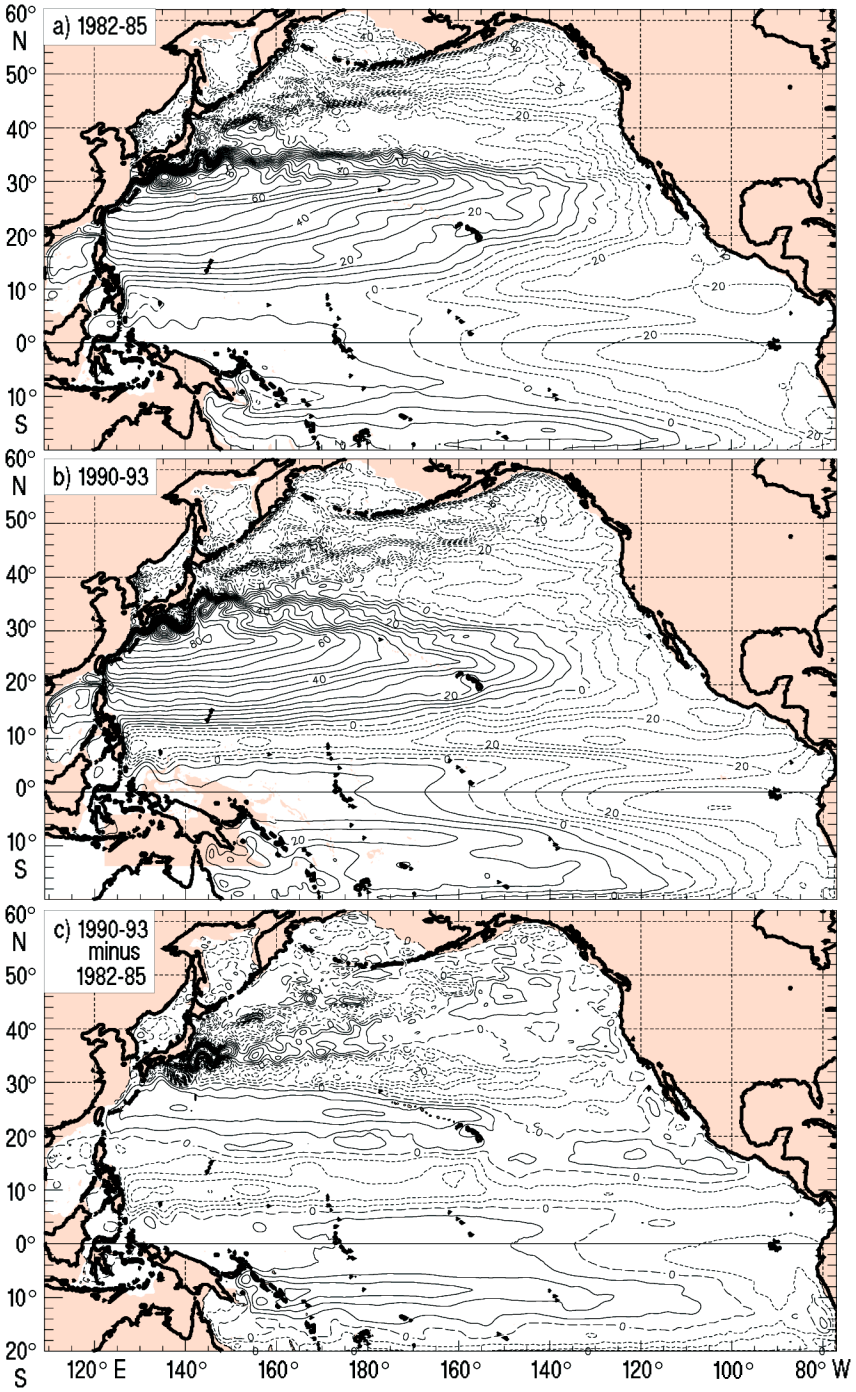

Fig. 22 — Sea-surface heights (SSH) simulated by a 1/8° six-layer Pacific Ocean model north of 20° S. The model is the NRL Layered Ocean Model (NLOM) forced by daily-averaged ECMWF 1000-mb archived operational winds with the long-term mean replaced by the Hellerman and Rosenstein (1983) (HR) annual mean. (a) 1982-1985 mean SSH, (b) 1990-1993 mean SSH, and (c) the change in mean SSH from 1982-1985 to 1990-1993 (mean from (b) minus the mean from (a)). The contour interval is 5 cm. For an extensive discussion of the Pacific Ocean model, see Hurlburt et al. (1996b). The results shown here are from simulation BT6 in Hurlburt et al. (1996).

trends are not corroborated by FSU. Smaller-scale and stronger topographically-induced wind features (due to ECMWF model resolution increases) cause these false strengthening trends. The scales of these wind features are possibly limited by subsampling to the 2.5° grid.

6.0 SUMMARY AND CONCLUSIONS

Monthly wind stress and wind stress curl computed from archived operational ECMWF 12-hrly 1000-mb global wind analyses and FSU pseudo stresses (mainly subjectively analyzed ship winds) have been compared over 1981-1993 in the tropical Pacific Ocean region (124° E-70° W, 29° S-29° N) to assess the ECMWF wind product. The FSU wind product was used as the standard for comparison because it was derived using the same procedures and data type throughout the 13-yr period. A comparison of three ratio maps (ECMWF 1000-mb/ECMWF 10-m, ECMWF 1000-mb/FSU and ECMWF 10-m/FSU) shows that the spatial variability in the height of the 1000-mb surface is negligible for this study. As part of this effort, the wind products are compared during 1982-1985 and 1990-1993 (encompassing the beginning and the end of the wind data time series) to study the effects of ECMWF product changes and to investigate the impact of TOGA TAO data (moored buoy array in the tropical Pacific) on the ECMWF wind analyses. ECMWF assimilated TOGA TAO data during 1990-1993 (predominantly after Nov 1992) to improve the wind analyses in the equatorial Pacific. TOGA TAO data was also used in the FSU wind analyses. A ratio, correlation, and energy analysis mainly comprise the wind product comparison and linear regression is used to determine the nature of trends in the ECMWF wind analyses. Over the study period, the ECMWF and FSU monthly wind stress and wind stress curl patterns are generally consistent with the basic NH and SH subtropical high pressure cells and the associated trade wind systems.

During 1982-1985, the ECMWF trade winds are 25-55% weaker than the FSU trade winds in the equatorial Pacific and temporal wind stress magnitude correlations at a given location are generally less than 0.50 in the eastern equatorial Pacific and range from 0.50-0.70 in the western equatorial Pacific. The $curl_z(\tau)$ is more diffuse in the ECMWF product in the NECC and northern tropical gyre region. The ECMWF trade wind magnitudes are twice as strong as the FSU trade wind magnitudes off the South American coast. The weak equatorial winds and strong coastal winds cause excessive convergence in the ECMWF product in comparison with FSU. The coastal wind pattern also produces a complex $curl_z(\tau)$ pattern which is not seen in the FSU product.

Around the Hawaiian Islands, the ECMWF wind field contains a curl dipole (positive $curl_z(\tau)$ to the north and negative $curl_z(\tau)$ to the south) due to the strong topographic influence in this product. Around the Central American coast, mountainous terrain with gaps produces localized features in the ECMWF product. These topographic features are not seen in the FSU product. The ECMWF product has a greater topographic influence than the FSU product because the ECMWF model has topography and the FSU pseudo stress observations are subjectively analyzed to a 2° * 2° grid from 2° * 10° binned data (smoothing localized wind features). A potential value of using models to assimilate data is demonstrated, namely, topographic effects, at least when the model resolution is sufficient.

During 1990-1993, the ECMWF and FSU equatorial trade wind magnitudes generally agree to within 20% and temporal correlations at a given location range from 0.50-0.70 across the equatorial Pacific. Strengthened and less diffuse $curl_z(\tau)$ in the ECMWF product in the NECC and northern tropical gyre region produces closer product agreement. This improved agreement in the wind stress and $curl_z(\tau)$ is due to the addition of TOGA TAO data in the ECMWF analyses (via data assimilation) as well as to other ECMWF product modifications. The upgrade to T213 is a likely contributor. The ECMWF equatorial trade wind strengthening is statistically significant but it is only partially corroborated by FSU. Therefore, the addition of TOGA/TAO data and the ECMWF product modifications have produced an unreal strengthening of the equatorial easterlies and consequently contributed to an unreal strengthening of the NECC and northern

tropical gyre in a 1/8° Pacific NLOM simulation forced with a derivative of these winds (hybrid winds). The much weaker trends in the FSU winds indicate that the ocean model response is not due to natural interannual variability. Off the South American coast, the ECMWF trade winds and $curl_z(\tau)$ are much weaker than in 1982-1985. The resulting reduced convergence agrees more closely with FSU. This weakening in the ECMWF product along the South American coast is statistically significant, but is not corroborated by the FSU product. This area is outside the TOGA TAO region and this change is not contemperaneous with the addition of TOGA TAO data. Timing suggests that the weakening ECMWF wind field here is due to ECMWF product modifications in the late 1980's. While this unreal weakening has improved the trade wind agreement along the coast, it has slightly worsened the agreement in the south central tropical Pacific. Statistically significant ECMWF trade wind strengthening in the western Pacific from 10°-25° N is partially corroborated by the FSU product. It causes slightly worse trade wind magnitude agreement over 1990-1993 vs. 1982-1985.

The curl dipole in the ECMWF wind field around the Hawaiian Islands and the localized wind features along the Central American coast become stronger and smaller in space scale due to the ECMWF model resolution increases. In regions of significant topography, the effects of model resolution changes are clearly seen. Statistically significant complicated trend patterns of $curl_z(\tau)$ are not corroborated by FSU. They are manifestations of smaller-scale and stronger curl features which occur due to ECMWF model resolution increases. Since a second ECMWF model resolution increase slightly decreased the size of the curl dipole around Hawaii, the ECMWF model resolution may still be too coarse and/or subsampling to the 2.5° grid may limit the effect of the model resolution increases on the subsampled product.

7.0 ACKNOWLEDGMENTS

This work has been performed as part of the 6.2 Global Ocean Prediction System project under program element 0602435N. This project is part of the Naval Ocean Modeling and Prediction (NOMP) program. We thank ECMWF and the National Center for Atmospheric Research (NCAR) for supplying the ECMWF analyses for this research and The Center for Ocean-Atmospheric Prediction Studies (COAPS) at FSU for supplying the FSU analyses. The ocean model simulation was performed by Pat Hogan on the Cray Y-MP/8128 at the Naval Oceanographic Office, Stennis Space Center, MS. We thank Amy Summers for preparing the figures.

8.0 REFERENCES

Atkinson, G. D., 1971: Forecaster's guide to tropical meteorology. USAF Air Weather Service, Technical Report No. 240, 341 pp.

Atkinson, G. D., and J. C. Sadler, 1970: Mean cloudiness and gradient-level-wind charts over the tropics. USAF Air Weather Service, Technical Report No. 215, vol. 1 text, vol. 2 charts.

Atlas, R., A. J. Busalacchi, M. Ghil, S. Bloom, and E. Kalnay, 1987: Global surface wind and flux fields from model assimilation of Seasat data. *J. Geophys. Res.*, **92**, 6477-6487.

Bengtsson, L., M. Kanamitsu, P. Kållberg, and S. Uppala, 1982: FGGE 4-dimensional data assimilation at ECMWF. *Bull. Amer. Meteor. Soc*., **63**, 29-43.

Cardone, V. J., G. Greenwood, and M. A. Cane, 1990: On trends in historical marine wind data. *J. Climate*, **3**, 113-127.

Chelton, D. B., A. M. Mestas-Nuñez, and M. H. Freilich, 1990: Global wind stress and Sverdrup circulation from the Seasat scatterometer. *J. Phys. Oceanogr.*, **20**, 1175-1205.

Davison, J., and D. E. Harrison, 1990. Comparison of Seasat scatterometer winds with tropical Pacific observations. *J. Geophys. Res.*, **95**, 3403-3410.

ECMWF, The Description of the ECMWF/WCRP Level III-A Global Atmospheric Data Archive, Technical Attachment, 1994: ECMWF, United Kingdom.

Fabrikant, A.L., J.L. Spiesberger, A. Silivra, and H.E. Hurlburt, 1998: Estimating climatic temperature change in the ocean with synthetic acoustic apertures. *J. IEEE Ocean Eng.*, **23**, 20-25.

Gill, A. E., 1982: *Atmosphere-Ocean Dynamics*. Academic Press, Inc., 662 pp.

Godfrey, J.S., 1989: A Sverdrup model of the depth-integrated flow for the world ocean allowing for island circulations. *Geophys. Astrophys. Fluid Dyn.*, **45**, 89-112.

Halpern, D., A. Hollingsworth, and F. Wentz, 1994: ECMWF and SSM/I global surface wind speeds. *Journal of Atmospheric and Oceanic Technology*, **11**, 779-788.

Harrison, D. E., 1989: On climatological monthly mean wind stress and wind stress curl over the world ocean. *J. Climate*, **2**, 57-70.

Hastenrath, S. 1985: *Climate and circulation of the tropics*. Kluwer Academic Publishers, 455 pp.

Hayes, S. P., L. J. Mangum, J. Picaut, A. Sumi, and K. Takeuchi, 1991: TOGA-TAO: A moored array for real-time measurements in the tropical Pacific Ocean. *Bull. Amer. Meteor. Soc.*, **72**, 339-347.

Hellerman, S., and M. Rosenstein, 1983: Normal monthly wind stress over the world ocean with error estimates. *J. Phys. Oceanogr.*, **17**, 1093-1104.

Hogan, P. J., H. E. Hurlburt, G. Jacobs, A. J. Wallcraft, W. J. Teague, and J. L. Mitchell, 1992: Simulation of GEOSAT, TOPEX/Poseidon, and ERS-1 altimeter data from a 1/8° Pacific Ocean model: Effects of space-time resolution on mesoscale sea surface height variability. *Mar. Tech. Soc. J.*, **22**, 98-107.

Hollingsworth, A. D., G. Shaw, P. Lonnbert, L. Illari, and A. J. Simmons, 1986: Monitoring of observation and analysis quality by a data assimilation system. *Mon. Weather Review*, **114**, 861-879.

Hurlburt, H.E. and E.J. Metzger, 1998: Bifurcation of the Kuroshio Extension at the Shatsky Rise. *J. Geophys. Res.*, **103**, 7549-7566.

Hurlburt, H. E., A. J. Wallcraft, Z. Sirkes, and E. J. Metzger, 1992: Modeling of the Global and Pacific Oceans: On the path to eddy-resolving ocean prediction. *Oceanography*, **5**, 9-18.

Hurlburt, H.E., M.R. Carnes, D.N. Fox, E.J. Metzger, O.M. Smedstad and A.J. Wallcraft, Eddy-resolving ocean modeling and prediction in the Pacific Ocean with assimilation of satellite altimeter and IR data, *Actes du Colloque Oceanographie Operationnelle et Observation Spatiale*, Biarritz, France, Meteo France, CNES, SMF, pp. 105-119, 1996a.

Hurlburt, H.E., A.J. Wallcraft, W.J. Schmitz Jr., P.J. Hogan, and E.J. Metzger, Dynamics of the Kuroshio/ Oyashio current system using eddy-resolving models of the North Pacific Ocean, *J. Geophys. Res.*, 101,941-976, 1996b.

Jacobs, G.A., H.E. Hurlburt, J.C. Kindle, E.J. Metzger, J.L. Mitchell, W.J. Teague, and A.J. Wallcraft, 1994: Decadal-scale trans-Pacific propagation and warming effects of an El Nino anomaly. *Nature*, **370**, 360-363.

Jacobs, G.A., W.J. Teague, J.L. Mitchell, and H.E. Hurlburt, 1996: An examination of the North Pacific Ocean in the spectral domain using Geosat altimeter data and a numerical ocean model. *J. Geophys. Res.* **101**, 1025-1044.

Lambert, S. J., 1988: A comparison of operational global analyses from the European Centre for Medium Range Weather Forecasts (ECMWF) and the National Meteorological Center (NMC). *Tellus*, **40A**, 272-284.

Ly, L. N., J. C. Kindle, J. D. Thompson, and W. J. Youtsey, 1992: Wind stress analysis over the western equatorial Pacific and North Atlantic Oceans based on ECMWF operational wind products, 1985-1989. Tech. Report TR-3, Institute for Naval Oceanography.

Mestas-Nuñez, A. M., D. B. Chelton, M. H. Freilich, and J. G. Richman, 1994: An evaluation of ECMWF-based climatological wind stress fields. *J. Phys. Oceanogr*., 24, 1532-1549.

Metzger, E. J., H. E. Hurlburt, J. C. Kindle, Z. Sirkes, and J. M. Pringle, 1992: Hindcasting of wind-driven anomalies using a reduced-gravity global ocean model. *Mar. Tech. Soc. J.*, **22**, 23-32.

Metzger, E. J., H.E. Hurlburt, G.A. Jacobs, and J.C. Kindle, 1994: Hindcasting wind-driven anomalies using reduced-gravity global models with 1/2 and 1/4 degree resolution. NRL Formal Report 7323--93-9444, 22 pp.

Mitchell, J.L., W.J. Teague, G.A. Jacobs, and H.E. Hurlburt, 1996: Kuroshio Extension dynamics from satellite altimetry and a model simulation. *J. Geophys. Res.,* **101**, 1045-1058.

Mitchum, G.T., 1995: The source of 90-day oscillations at Wake Island. *J. Geophys. Res.*, 100(C2), 2459-2475.

Munk, W.H., 1950: On the wind-driven ocean circulation. *J. Meteorol.*, 7, 79-93.

Reynolds, R. W., K. Arpe, C. Gordon, S. P. Hayes, A. Leetmaa, and M. J. McPhadden, 1989: A comparison of tropical Pacific surface wind analyses. *J. Climate*, **2**, 105-111.

Rienecker, M. M., R. Atlas, S. D. Schubert, and C. S. Willett, 1996: A comparison of surface wind products over the North Pacific Ocean. *J. Geophys. Res.*, **101**, 1011-1023.

Sadler, J. C., 1975: The upper tropospheric circulation over the global tropics. Department of Meteorology, University of Hawaii, UHMET-75-05, 35 pp.

Shriver, J.F., 1993: Interdecadal variability of the equatorial Pacific Ocean and atmosphere: 1930-1989. Technical report. Mesoscale Air-Sea Interaction Group. The Florida State University, Tallahassee, FL, 97 pp.

Silivra, A.A., J.L. Spiesberger, A.L. Fabrikant, and H.E. Hurlburt, 1997: Acoustic tomography at basin-scales and clock errors. *J. IEEE Ocean Eng.*, **22**, 143-150.

Smedstad, O.M., D.N. Fox, H.E. Hurlburt, G.A. Jacobs, E.J. Metzger, and J. Mitchell, 1997: Altimeter data assimilation into a 1/8E eddy resolving model of the Pacific Ocean. *J. Met. Soc. Japan*, **75**, 429-444. (Invited).

Spiesberger, J.L., A. Fabrikant, A. Silivra, and H.E. Hurlburt, 1997: Mapping climatic temperature changes in the ocean with acoustic tomography: Navigational requirements. *J. IEEE Ocean Eng*., **22**, 128-142.

Spiesberger, J.L., H.E. Hurlburt, M.A. Johnson, M. Keller, S.D. Meyers, and J.J. O'Brien, 1998: Acoustic thermometry data compared with two ocean models: the importance of Rossby waves and ENSO in modifying the ocean interior. *Dyn. Atmos. Ocean.*, **26**, 209-240.

Stommel, H., 1948: The western intensification of wind-driven currents. *Trans. Amer. Geophys. Union*, 29, 202-206.

Stricherz, J. N., J. J. O'Brien, and D. M. Legler, 1992: Atlas of Florida State University tropical Pacific winds for TOGA 1966-1985, Florida State University, Tallahassee, FL, 275 pp.

Sverdrup, H.E., 1947: Wind-driven currents in a baroclinic ocean; With application to the equatorial currents of the eastern Pacific. *Proc. Natl. Acad. Sci.* U.S.A., 33, 318-326.

Thompson, J. D., T. L. Townsend, A. Wallcraft, and W. J. Schmitz, Jr., 1992: Ocean prediction and the Atlantic basin: Scientific issues and technical challenges. *Oceanography*, **5**, 36-41.

Trenberth, K. E., and J. G. Olson, 1988: An evaluation and intercomparison of global analyses from the National Meteorological Center and the European Centre for Medium Range Weather Forecasts. *Bull. Amer. Meteor. Soc.*, **69**, 1047-1057.

Trenberth, K.E., J. G. Olson and W. G. Large, 1989: A global ocean wind stress climatology based on ECMWF analyses. NCAR Tech. Note NCAR/TN-338+STR, 93 pp.

Trenberth, K.E., W.G. Large, and J. G. Olson, 1990: The mean annual cycle of the global ocean wind stress. *J. Phys. Oceanogr.*, **20**, 1742-1760.

Trenberth, K.E., 1992: Global analyses from ECMWF and atlas of 1000 to 10 mb circulation statistics. NCAR Tech. Note. NCAR/TN-373+STR, 191 pp.

Appendix A

ECMWF WIND STRESS IN THE PACIFIC OCEAN AND ATLANTIC/INDIAN OCEAN DOMAINS

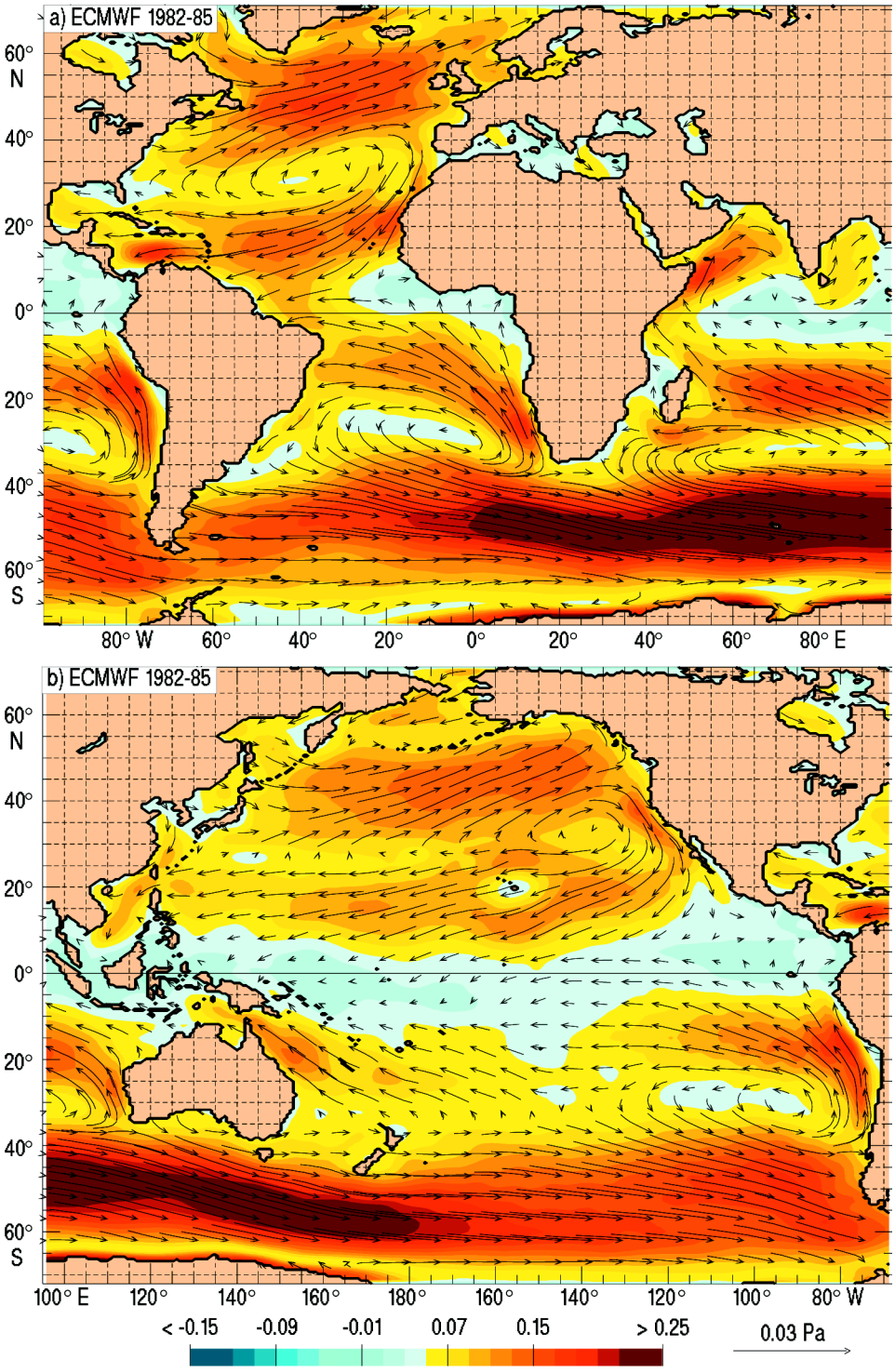

Fig. A1 — ECMWF mean wind stress magnitude for 1982-1985 for (a) Atlantic domain and (b) Pacific domain. Wind stress vectors are overlaid on the wind stress magnitude. Contour interval is 0.020 Pa.

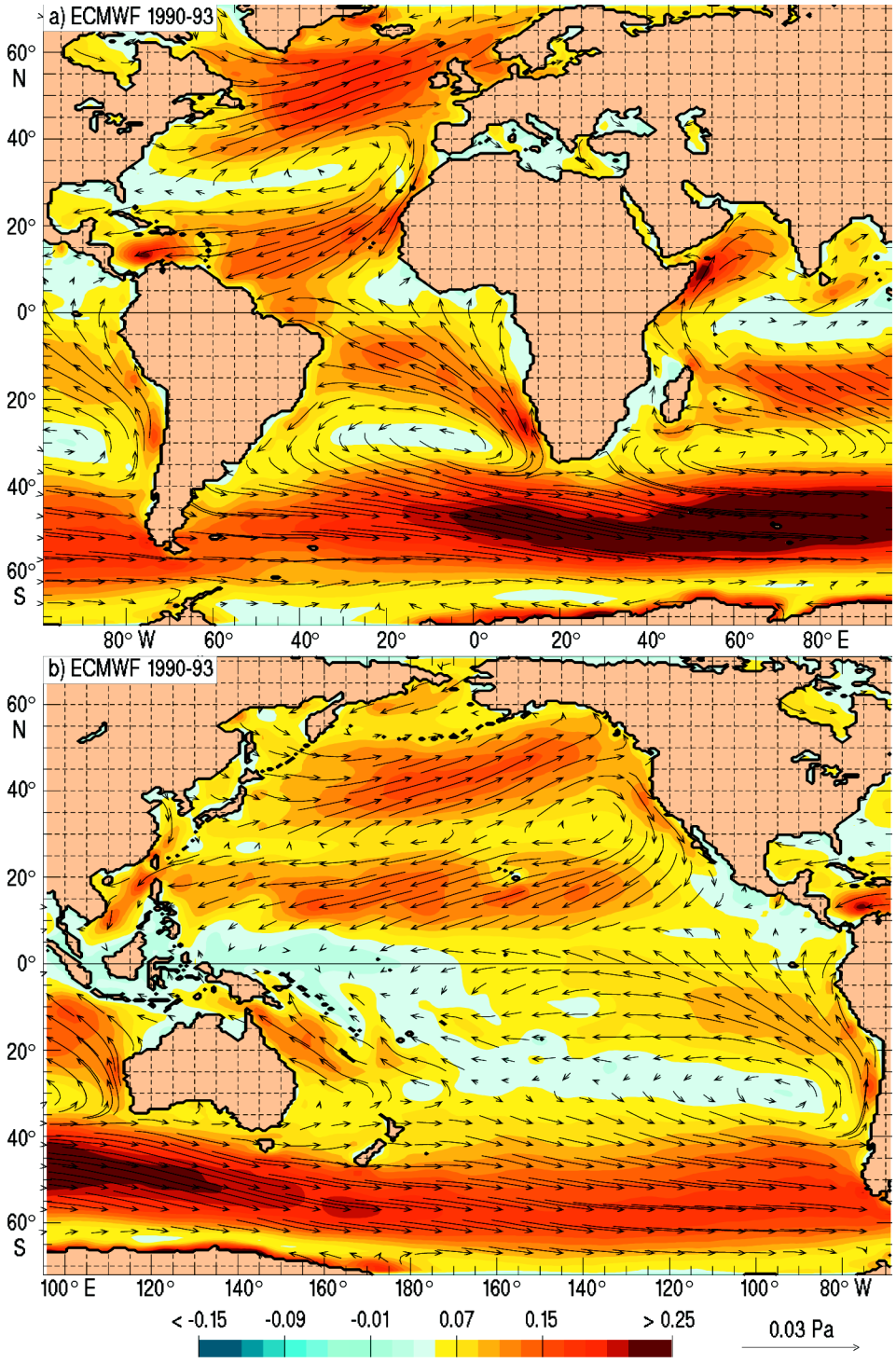

Fig. A2 — Same as Fig. A1, except showing 1990-1993

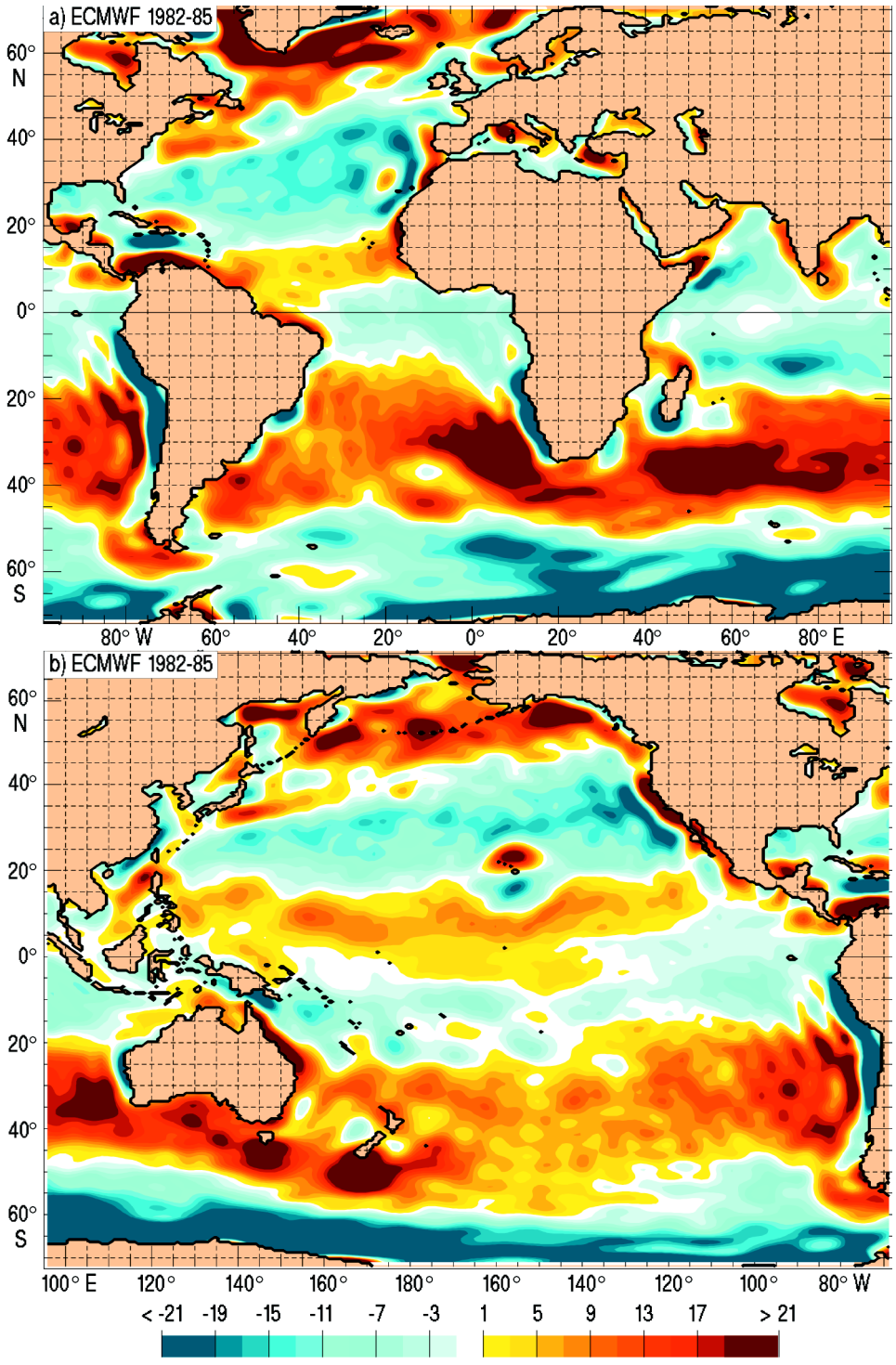

Fig. A3. ECMWF mean wind stress curl for 1982-1985 for (a) Atlantic domain and (b) Pacific domain. Yellow shades indicate positive wind stress curl and blue shades indicate negative wind stress curl. Zero or near zero wind stress curl lines are white. The contour interval is 2 * 10^{-8} Pa/m. The values are scaled by 10^{8} on the color bar.

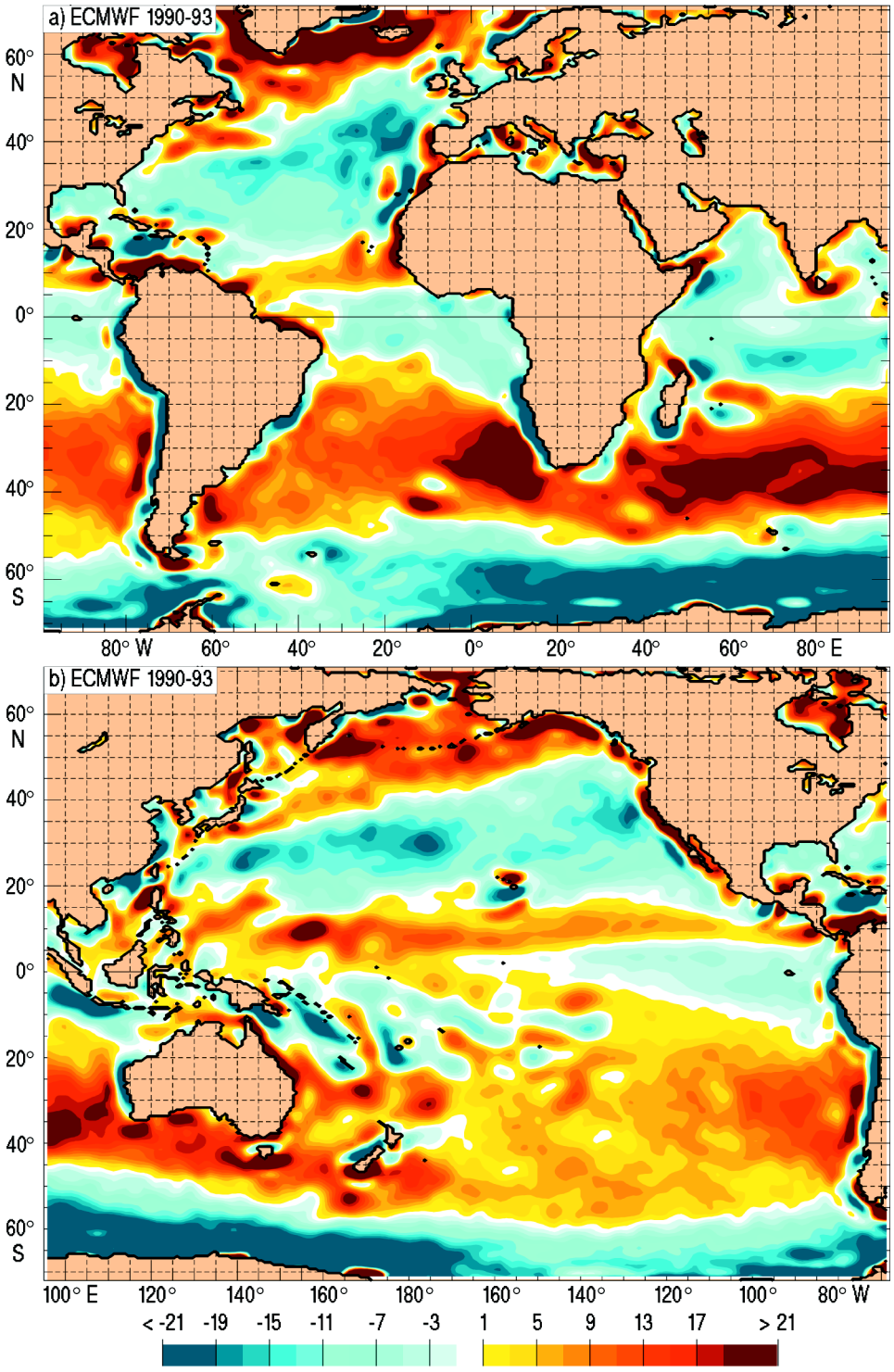

Fig. A4 — Same as Fig. A3, except showing 1990-1993

Appendix B

ECMWF 1000-MB/10-M WIND STRESS MAGNITUDE RATIOS

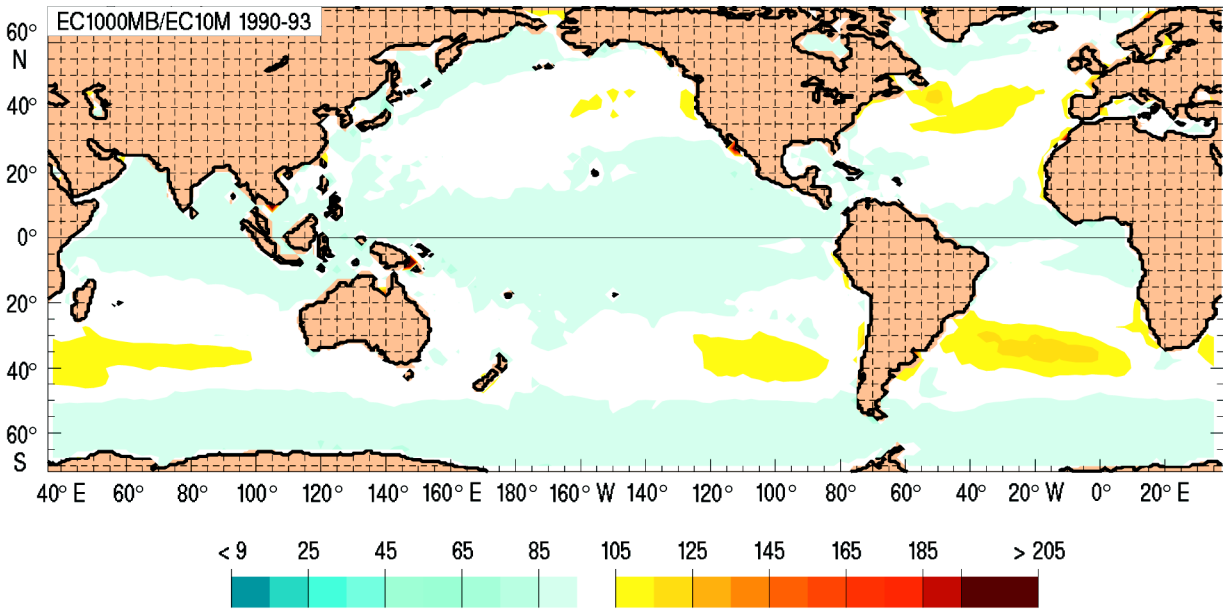

Fig. B1 — The ratio of wind stress magnitudes calculated from the ECMWF 1000-mb winds and the ECMWF 10-m winds for 1990-1993. The ECMWF 10-m winds at each gridpoint were normalized by the spatially averaged ECMWF 1000- mb/ECMWF 10-m wind stress magnitude ratio. Ratio values are multiplied by 100. Blue shades indicate weaker ECMWF 1000-mb wind stress magnitudes and yellow shades indicate stronger ECMWF 1000-mb wind stress magnitudes. White indicates equal or nearly equal values. The contour interval is 10.

Appendix C

REGRESSION COEFFICIENTS AND STATISTICAL SIGNIFICANCE FOR THE ECMWF WIND STRESS

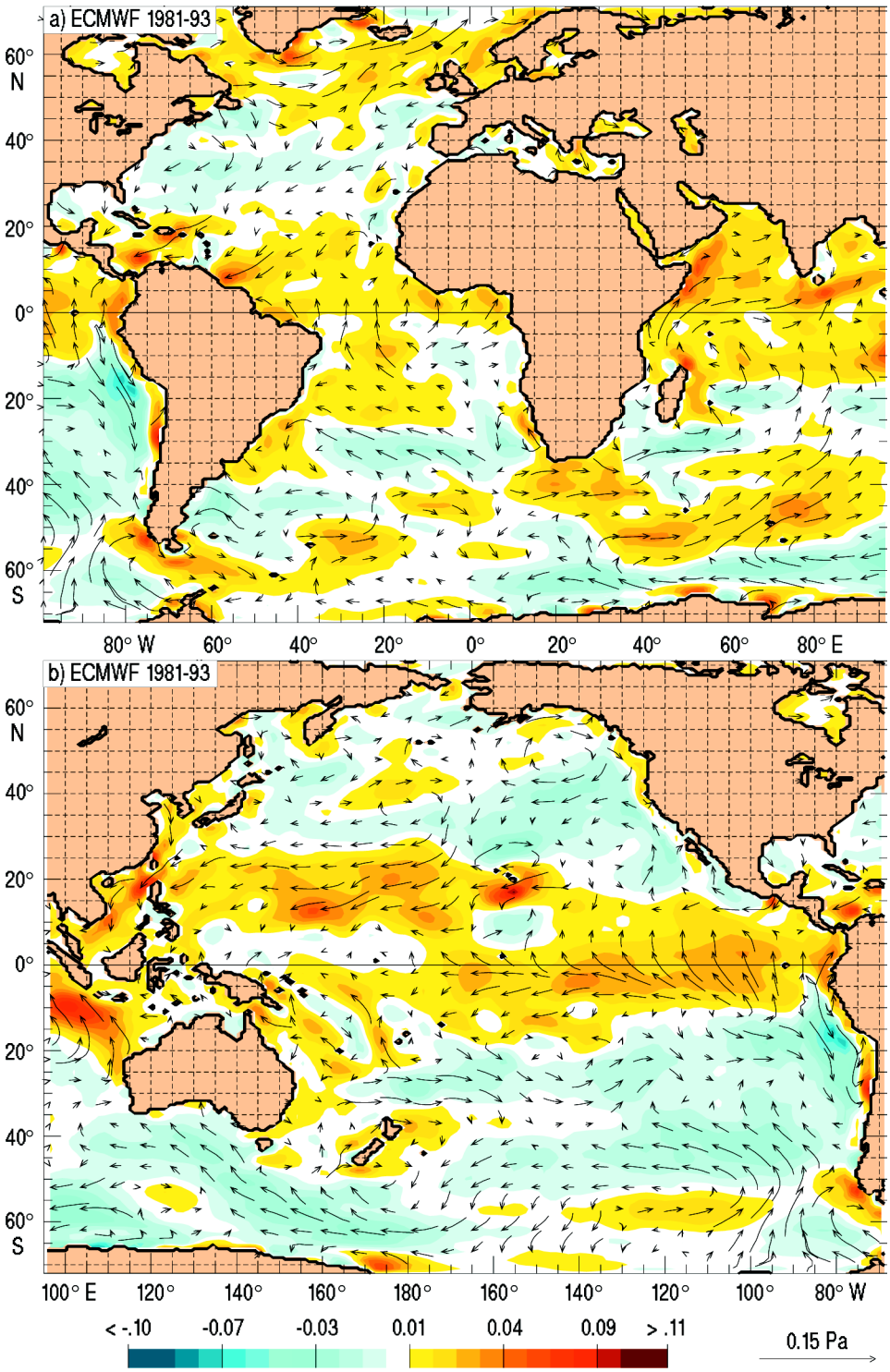

Fig. C1 — Regression coefficients for ECMWF wind stress magnitude for (a) Atlantic domain and (b) Pacific domain. Trends in wind stress magnitude are displayed as color contours. Trends in the wind stress components are shown as overlaid arrows. Yellow shades indicate a strengthening trend and blue shades indicate a weakening trend. White indicates a zero or near zero trend. The contour interval is 10^{-4} Pa/month. The values are multiplied by 100 on the color bar.

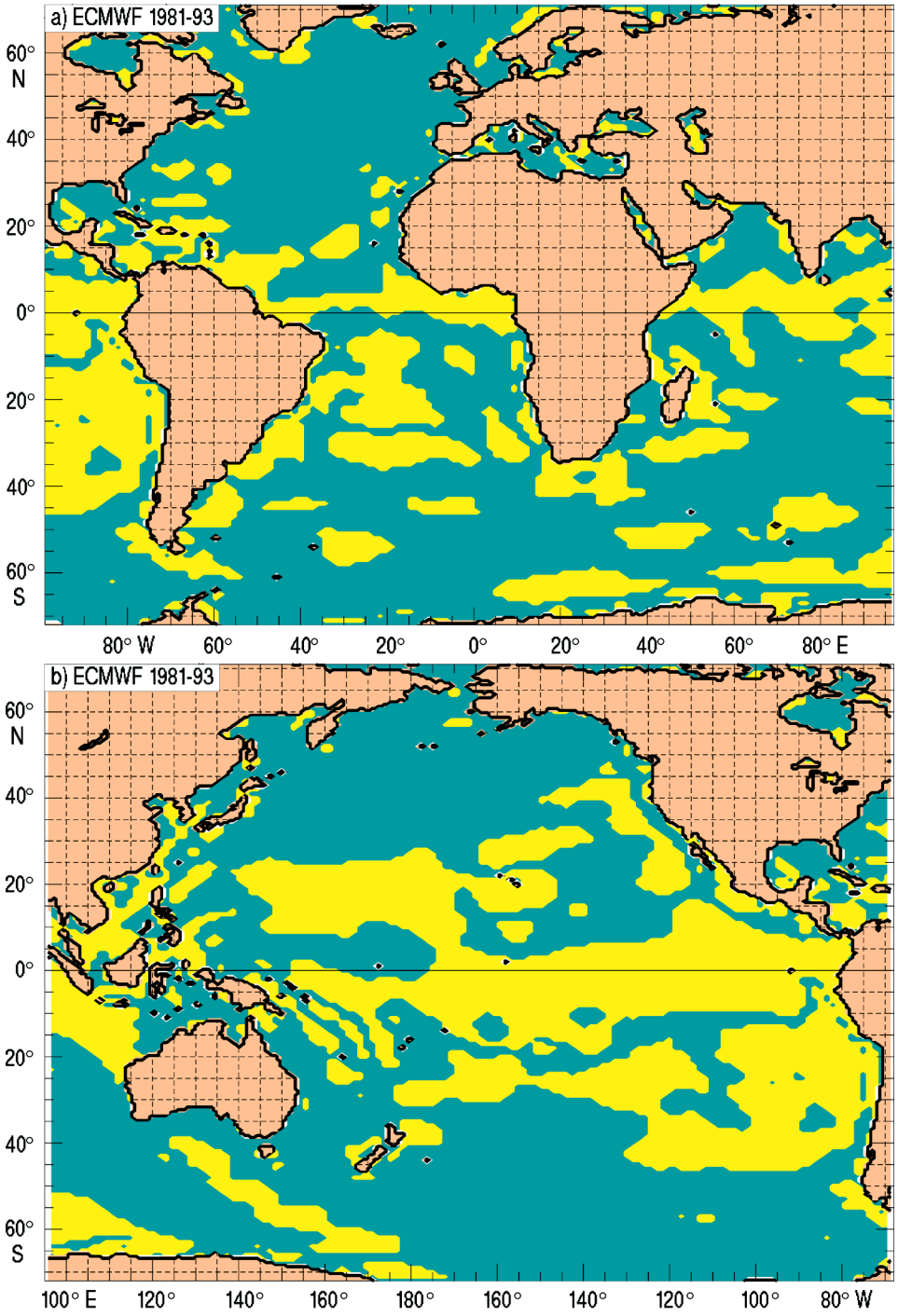

Fig. C2 — Statistical significance of the ECMWF wind stress regression coefficients for (a) Atlantic domain and (b) Pacific domain. The statistical significance was calculated using Student's t-test at the 95% confidence level. Yellow indicates statistical significance while blue indicates statistical insignificance.

Appendix D

REGRESSION COEFFICIENTS AND STATISTICAL SIGNIFICANCE FOR THE ECMWF WIND STRESS CURL

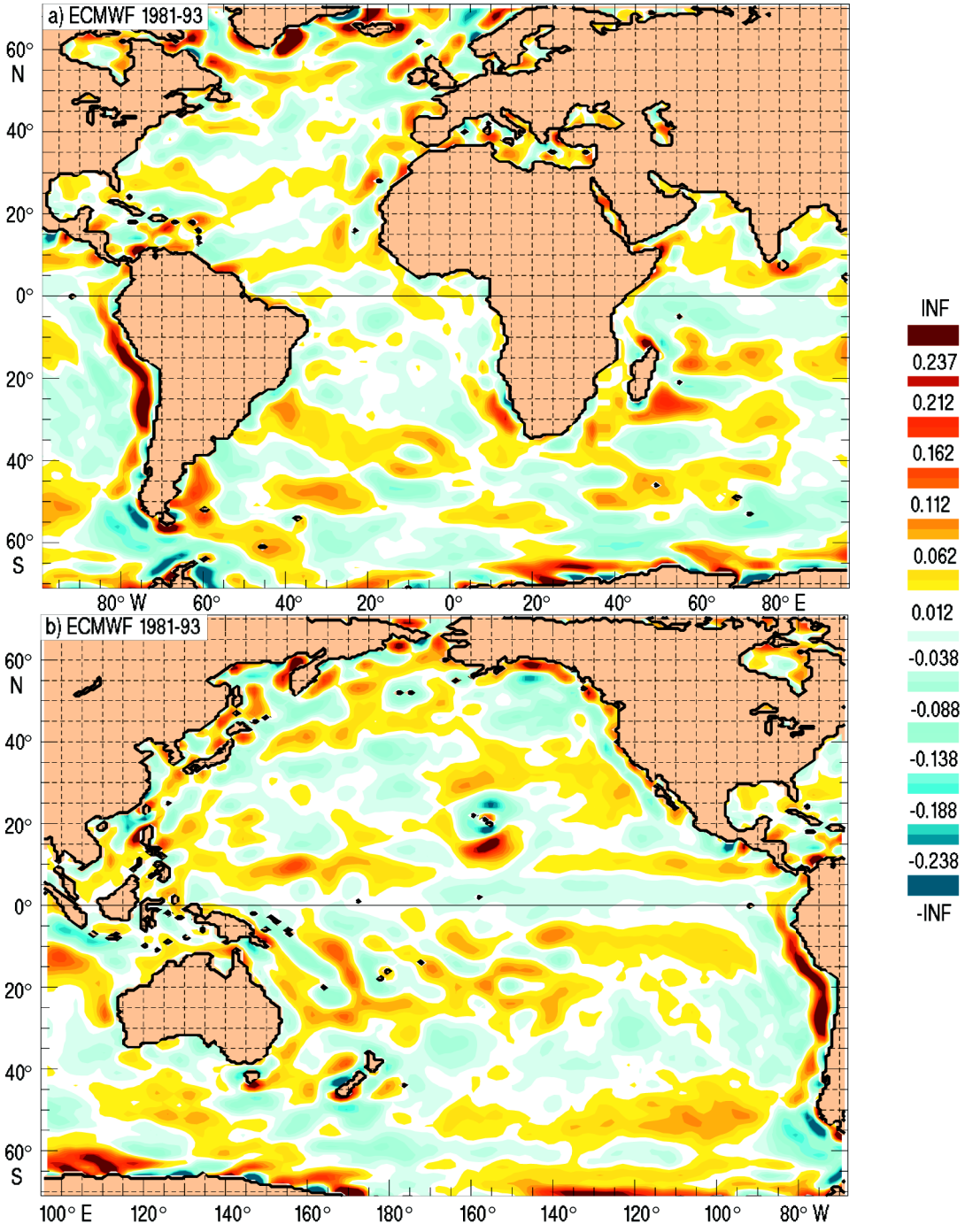

Fig. D1 — Regression coefficients for ECMWF wind stress curl for (a) Atlantic domain and (b) Pacific domain. Yellow shades indicate an increasing trend and blue shades indicate a decreasing trend. White indicates a zero or near zero trend. The contour interval is 2.5 * 10^{-10} Pa/m*month. Values are scaled by 10^{8} on the color bar.

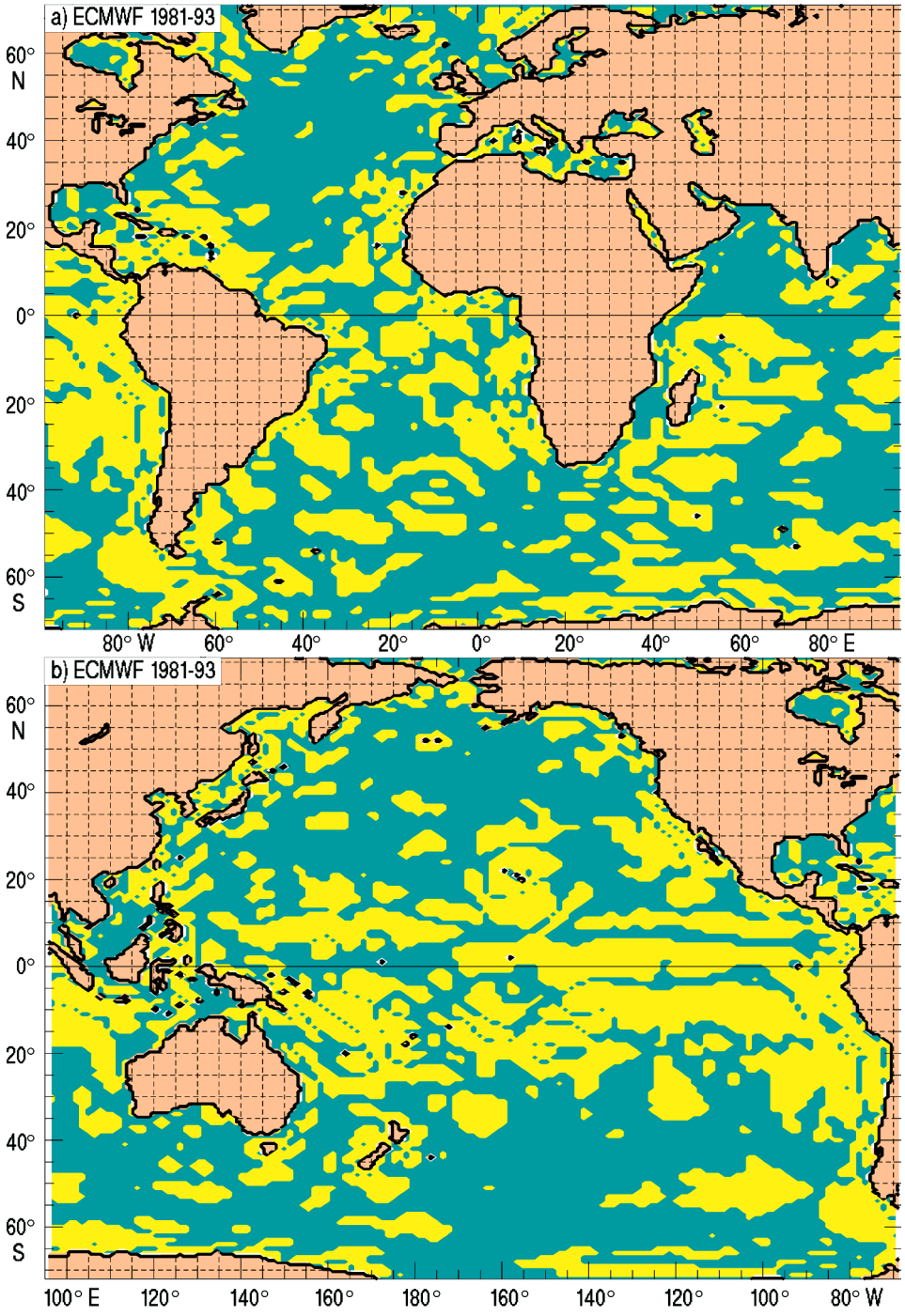

Fig. D2 — Statistical significance of the ECMWF wind stress curl regression coefficients for (a) Atlantic domain and (b) Pacific domain. The statistical significance was calculated using Student's t-test at the 95% confidence level. Yellow indicates statistical significance while blue indicates statistical insignificance.